Confined hydrogenlike ions in plasma environments

Neetik Mukherjee,[1,*] Chandra N. Patra,[2,†] and Amlan K. Roy[1,‡]
[1]*Department of Chemical Sciences, IISER Kolkata, Mohanpur 741246, Nadia, West Bengal, India*
[2]*Theoretical Chemistry Section, Chemistry Group, Bhabha Atomic Research Centre, Mumbai 400085, India*

(Received 27 April 2021; accepted 21 June 2021; published 8 July 2021)

The behavior of H-like ions embedded in astrophysical plasmas in the form of *dense, strongly and weakly coupled* plasmas is investigated. In these, the increase and decrease in temperature are impacted by a change in confinement radius r_c. Two independent and generalized scaling ideas have been applied to modulate the effect of the plasma-screening constant λ and ion charge Z on such systems. Several relations are derived to interconnect the original Hamiltonian and two scaled Hamiltonians. In the exponential-cosine-screened Coulomb potential (ECSCP; dense) and weakly coupled plasma (WCP) these scaling relations have provided a linear equation connecting the critical screening constant $\lambda^{(c)}$ and Z. Their ratio offers a state-dependent constant beyond which a particular state vanishes. Shannon entropy has been employed to understand the plasma effect on the ion. With an increase in λ, the accumulation of opposite charge surrounding the ion increases, leading to a reduction in the number of bound states. However, with a rise in ionic charge Z, this effect can be delayed. The competing effect of plasma charge density n_e and temperature in WCP and ECSCP is investigated. A recently proposed simple virial-like theorem was established for these systems. Multipole ($k = 1$–4) oscillator strength and polarizabilities for these are studied considering $1s$, $2s$ states. As a bonus, analytical closed-form expressions are derived for $f^{(k)}$ and $\alpha^{(k)}(k = 1$–$4)$ involving $1s$ and $2s$ states for the *free H-like ion*.

DOI: 10.1103/PhysRevA.104.012803

I. INTRODUCTION

The discovery and development of quantum confinement [1,2] has triggered the study of the influence of environment on quantum systems. In confined conditions, rearrangement of orbitals may occur in atoms and molecules, leading to some fascinating changes in physical and chemical properties. Especially, this leads to an increase in the coordination number of atoms [3], enhanced reactivity of atoms and molecules, room-temperature superconductivity [4], etc. The environment-driven confinement has profound applications in condensed-matter, semiconductor physics, astrophysics, nanotechnology, etc. In this context, the influence of the plasma environment [5–7] in astrophysical systems is a subject of topical interest. Particularly, the impact of the charge cloud and temperature on bound quantum states can be determined by investigating atoms and ions trapped inside various plasma environments [8–10].

In such conditions, the competing effects of plasma free-electron density n_e and temperature T_e play a pivotal role in stabilizing the bound states of a given system. The plasma coupling parameter Γ is expressed as [11]

$$\Gamma = \frac{E_{\text{coulomb}}}{E_{\text{thermal}}} = \frac{Q^2}{4\pi\epsilon_0 a k_b T_e}. \tag{1}$$

Here, Q denotes the charge on the particle, inner particle separation is given by $a = (\frac{3}{4\pi n_e})^{\frac{1}{3}}$, k_b signifies Boltzmann's constant, and n_e refers to plasma electron density. Depending on the value of Γ, the following two situations may be envisaged.

(1) $\Gamma < 1$ arises for low-density and high-temperature or weakly coupled plasma (WCP). The thermal energy is higher than the Coulomb energy in this case.

(2) $\Gamma > 1$ occurs for strongly coupled plasma (SP). It has high density and low temperature. The thermal energy is now lower than the Coulomb energy. This type of plasma has been produced experimentally.

In hot WCP, the collective screening effect of plasma on the electron-charged particle interaction is assumed to behave as the Debye-Hückel potential, expressed in the form $V_1(r) = -\frac{Z}{r}e^{-\lambda_1 r}$. Here, $\lambda_1 = \sqrt{\frac{4\pi e^2 n_e}{k_b T_e}}$ corresponds to the inverse of Debye radius D. The screening parameter arises due to the surrounding plasma cloud. In the last two decades, this system has been studied vigorously with immense interest. The impact of the plasma-screening effect on the energy spectrum [12–15], inelastic electron-ion scattering [16,17], two-proton transitions [18,19], and transition probabilities involving electron-impact excitation [20–22], information entropy (Shannon entropy, Fisher information, and statistical complexities) [23], etc., has been investigated. The dynamic plasma-screening effect was considered in [24–27]. The relativistic correction to the plasma-screening effect was also explored [28]. Various spectroscopic properties, including multipole oscillator strength (OS) and static multipole polarizabilities, were calculated for H-like

*pchem.neetik@gmail.com
†chandra@barc.gov.in
‡Corresponding author: akroy@iiserkol.ac.in; akroy6k@gmail.com

atoms embedded in WCP [29–33] using several numerical methods. A time-dependent variation perturbation method was employed to calculate transition probabilities, OS, and static dipole polarizabilities for the ground state at different λ_1 values [34]. The numerical symplectic-integration method [30–32], mean-excitation-energy-based approximation formula [33], integration-based shooting technique [35], linear-variation method [36], etc., were also employed to extract these spectroscopic properties. The hyperpolarizability of H atoms under spherically confined Debye plasma was reported in [37]. Recently, polarizabilities were also computed for confined WCP plus ring-shaped potentials [38]. A closed-form expression for the critical screening constant in the ground state of WCP was proposed in [39]. Numerical values for ground and low-lying excited states were reported in [40]. Recently, a generalized pseudospectral (GPS) method was used in computing OS and polarizabilities in ground and excited states ($\ell = 0$) [8]. In all these cases, calculations were mostly concentrated in estimating the dipole OS and polarizabilities considering $1s$ as the initial state. However, WCP in a *confined* condition with varying λ_1 has not yet been well explored. It remains one of the primary objectives of this paper.

The composite screening and wake effect around a slow-moving test charge in low-density quantum plasma are mimicked by using an exponential-cosine-screened Coulomb potential (ECSCP), having the form $V_2(r) = -\frac{Z}{r}e^{-\lambda_2 r}\cos\lambda_2 r$. Here, $\lambda_2 = \frac{k_q}{\sqrt{2}} = \sqrt{\frac{n_e\omega_{pe}}{\hbar}}$ signifies the screening parameter, and k_q is the electron plasma wave number connected to electron plasma frequency and number density. The cosine term in this model is introduced under the assumption that the quantum force acting on plasma electrons predominates over the statistical pressure of plasmas [10,41]. A variety of theoretical methods like the perturbation-and-variation method [42], Padé scheme [43], shooting method [44], Supersymmetric (SUSY) perturbation method [45], asymptotic iteration [46], variation using hydrogenic wave functions [47], J matrix [48], symplectic integration [49], GPS [50], basis-expansion method with Slater-type orbitals [51], Laguerre polynomials [52], etc., were employed to extract the eigenvalue and eigenfunctions of this system. Similarly, the influence of λ_2 on the energy spectrum [14,15], electron-impact excitation [22], photoionization cross section [52,53], etc., was discussed in appreciable detail. Apart from that, polarizabilities were also evaluated for confined ECSCP plus a ring-shaped potential [38]. A relativistic correction to the screening effect was also explored. Further, the laser-induced excitation on a confined H atom in ECSCP was pursued using the Bernstein-polynomial method [54]. In this context, the impact of the shape of laser pulse, r_c, λ_2, and various laser parameters on the dynamics of the system has been examined and analyzed. Several attempts were made to estimate the characteristic value of λ_2 at which a bound state designated by quantum numbers n, ℓ disappears [39]. The critical screening parameters for $n \leqslant 6$ and $0 \leqslant \ell \leqslant n-\ell$ were accurately estimated in Ref. [55]. The dipole OS and polarizabilities at various λ_2 values were reported before in Refs. [44,45,49,51,56]. Recently, the utility of the GPS method in ECSCP [10] was examined by evaluating OS and polarizabilities. But here again, barring a few exceptions, the majority of the calculations have focused on the ground state. Moreover, to the best of our knowledge, ECSCP in a *confined* environment has not been probed so far in a sufficiently thorough manner.

In SP [5], an ion experiences the plasma effect within the ion-sphere radius R. Thus, no electron current moves through the boundary surface. It is generally described by a potential of the form [35]

$$V_3(r) = \begin{cases} -\frac{Z}{r} + \left(\frac{Z-N_e}{2R}\right)\left[3 - \left(\frac{r}{R}\right)^2\right], \\ 0 \quad r > r_c = R, \end{cases} \tag{2}$$

where $R = [\frac{3(Z-N_e)}{4\pi n_e}]^{\frac{1}{3}}$. The free electrons in an ion sphere distribute uniformly. The *ion-sphere* model is profoundly useful and expected to be valid in the limit of low temperature and high density. Several theoretical methods have been employed to understand the effect of SP on energy levels and wave functions of H-like atoms [57–59]. Moreover, atomic transition probabilities [60], transition energies and polarizabilities [35], photoionization and the photoionization cross section [11,61], OS and static polarizabilities [62], etc., in this case were studied previously. However, akin to the earlier two cases (WCP and ECSCP), most of the works have been restricted to only the ground state.

We have a number of objectives in this article. First, a detailed investigation is made of the three plasma conditions, viz., WCP, ECSCP, and SP, with special emphasis on their confinement situation and excited states, for which the literature results are quite scarce. It may be noted that the influence of the physical situation governed by a potential of the form $V = \infty$ at $r > r_c$ in the context of plasma has not been considered before. In addition, its significance and relation to the plasma environment are also not very clear. Here, the confined condition is mapped with *plasma temperature*. It may be noted that the multipole OS and polarizabilities of the H atom in various plasmas have been reported in a number of publications. However, such works in the confined scenario, as implied above, have not been considered before. Thus, a secondary objective is to examine the *effect of confinement* on multipole OS and polarizabilities for WCP, ECSCP, and SP. Two different scaling ideas connecting λ and Z are formulated. The relation between these two individual concepts is derived and explained. Additionally, Shannon entropy S has been invoked to determine the critical screening constant in *free* WCP and ECSCP. Our results show this can be an interesting route. Beyond this critical parameter (the binding energy of a given state disappears), no bound states could be found. After some debate, It is now a well-accepted fact that the standard form of the virial theorem (VT) is not ordinarily obeyed in enclosed conditions. An appropriate modified form is invoked in Ref. [63], which holds well in both free and confined conditions. The utility and efficiency of this relation are examined in the context of the plasma environment.

Thus, we have performed detailed calculations of multipole OS ($k = 1$–4) and polarizabilities in the $1s$, $2s$ states of WCP, ECSCP, and SP employing accurate GPS wave functions. Here, $k = 1$–4 represent dipole, quadrupole, octupole, and hexadecapole transitions, respectively. In WCP and ECSCP, we demonstrate the spectroscopic properties in two different

ways. First, they are calculated by varying λ, keeping r_c fixed. Second, the impact of the variation of r_c on these properties at fixed λ is also verified. Analogous calculations are done in SP, with a change in r_c. As a bonus, some analytical closed-form expressions of multipole OS (up to hexadecapole) and polarizabilities (up to hexadecapole) are derived for the $1s$, $2s$ states of a *free H atom* (FHA). In the literature, these forms are available in only in the *dipole case*. This article is organized in the following parts: Sec. II presents a brief description of the formalism employed in the current work. In Sec. III, the connection between plasma temperature and quantum confinement is proposed and explained. Section IV provides a detailed discussion of the results for WCP, ECSCP, and SP. Finally, we conclude with a few remarks and future prospects in Sec. V.

II. THEORETICAL FORMALISM

The time-independent radial Schrödinger equation (SE) for the spherically confined plasma system is expressed as (in atomic units)

$$\left[-\frac{1}{2}\frac{d^2}{dr^2}+\frac{\ell(\ell+1)}{2r^2}+V_c(r)+V_0\,\theta(r-r_c)\right]\psi_{n,\ell}(r) = \mathcal{E}_{n,\ell}\,\psi_{n,\ell}(r). \tag{3}$$

Here, V_0 is a positive number with a numerical value approaching ∞, and $\theta(r-r_c)$ is a Heaviside function that reaches 1 at $r=r_c$ and is *zero* otherwise, whereas $V_c(r)$ represents the various plasma potentials discussed later in this section. To calculate the energy and spectroscopic properties, the GPS method has been exploited. Over time, its accuracy and efficiency in calculating various bound-state properties in several central potentials in both free and confined conditions have been verified and established (see [63–68] and references therein). In what follows, atomic units (a.u.) are employed unless otherwise mentioned.

A. Virial-like theorem

Recently, a virial-like relation was proposed for free and confined quantum systems by invoking the time-independent nonrelativistic SE and hypervirial theorem [63]. The generalized form of this equation is expressed as

$$\langle\hat{T}^2\rangle_n-\langle\hat{T}\rangle_n^2=\langle\hat{V}^2\rangle_n-\langle\hat{V}\rangle_n^2. \tag{4}$$

$\hat{T}$ and $\hat{V}$ represent the kinetic- and potential-energy operators, respectively. Further, $(\Delta\hat{T})^2=\langle\hat{T}^2\rangle-\langle\hat{T}\rangle^2$ and $(\Delta\hat{V})^2=\langle\hat{V}^2\rangle-\langle\hat{V}\rangle^2$ signify their standard deviations. Equation (4) can be used as a necessary condition for an exact quantum system to obey. Further, it has been proved that the equation

$$(\Delta\hat{T}_n)^2=\langle\hat{V}\rangle_n\langle\hat{T}\rangle_n-\langle\hat{T}\hat{V}\rangle_n=(\Delta\hat{V}_n)^2 = \langle\hat{T}\rangle_n\langle\hat{V}\rangle_n-\langle\hat{V}\hat{T}\rangle_n \tag{5}$$

can act as a sufficient condition for a bound, stationary state [63]. Moreover, an alteration in boundary conditions does not influence the general form. Equations (4) and (5) are applicable in all coordinate systems, such as ellipsoidal, parabolic, cylindrical, spheroidal, etc. Equations (4) and (5) are obeyed in both free and confined conditions in unconfined and confined systems (including angular confinement). In the present endeavor, this has been extended to the plasma environment.

B. Multipole polarizabilities

The static multipole polarizabilities can be expressed in following form:

$$\alpha_i^{(k)}=\alpha_i^{(k)}(\text{bound})+\alpha_i^{k}(\text{continuum}). \tag{6}$$

It is customary to write $\alpha_i^{(k)}$ in terms of the compact sum-over-states form [35]. However, it can also be directly computed by adopting the standard perturbation-theory framework [69]. In the former procedure, Eq. (5) is modified to

$$\alpha_i^{(k)}=\sum_n\frac{f_{ni}^{(k)}}{(\mathcal{E}_n-\mathcal{E}_i)^2}-c\int\frac{|\langle R_i|r^kY_{kq}(\mathbf{r})|R_{\epsilon p}\rangle|^2}{(\mathcal{E}_{\epsilon p}-\mathcal{E}_i)}\,d\epsilon,$$
$$\alpha_i^{(k)}(\text{bound})=\sum_n\frac{f_{ni}^{(k)}}{(\Delta\mathcal{E}_{ni})}, \tag{7}$$
$$\alpha_i^{k}(\text{continuum})=c\int\frac{|\langle R_i|r^kY_{kq}(\mathbf{r})|R_{\epsilon p}\rangle|^2}{(\mathcal{E}_{\epsilon p}-\mathcal{E}_i)}\,d\epsilon.$$

In Eq. (6), the summation and integral terms represent the bound and continuum contributions, respectively, $f_{ni}^{(k)}$ signifies the multipole OS (k is a positive integer), and c is a constant which depends on the ℓ quantum number. $f_{ni}^{(k)}$ measures the mean probability of transition between an initial state i and a final state n, which is normally expressed as

$$f_{ni}^{(k)}=\frac{8\pi}{(2k+1)}\Delta\mathcal{E}_{ni}|\langle r^kY_{kq}(\mathbf{r})\rangle|^2. \tag{8}$$

Designating the initial and final states as $|n\ell m\rangle$ and $|n'\ell'm'\rangle$, one can easily derive

$$f_{ni}^{(k)}=\frac{8\pi}{(2k+1)}\,\Delta\mathcal{E}_{ni}\,\frac{1}{2\ell+1} \times\sum_m\sum_{m'}|\langle n'\ell'm'|r^kY_{kq}(\mathbf{r})|n\ell m\rangle|^2. \tag{9}$$

The application of the Wigner-Eckart theorem and sum rule for the $3j$ symbol further leads to

$$f_{ni}^{(k)}=2\,\frac{(2\ell'+1)}{(2k+1)}\,\Delta\mathcal{E}_{ni}\,\left|\langle r^k\rangle_{n\ell}^{n'\ell'}\right|^2\begin{Bmatrix}\ell' & k & \ell\\ 0 & 0 & 0\end{Bmatrix}^2. \tag{10}$$

The transition matrix element is expresses by the radial integral,

$$\langle r^k\rangle=\int_0^\infty R_{n'\ell'}(r)r^kR_{n\ell}(r)r^2dr. \tag{11}$$

Thus, it is clear that $f_{ni}^{(k)}$ depends on n, ℓ quantum numbers, while being independent of the magnetic quantum number m. In this article, we aim to compute multipole ($k=1$–4) polarizabilities and OS for the $1s$, $2s$ states. The corresponding selection rule for the dipole OS ($k=1$) for these two states is ($i=1$ or 2)

$$f_{np-is}^{(1)}=2\,\Delta\mathcal{E}_{np-is}\left|\langle r\rangle_{is}^{np}\right|^2\begin{Bmatrix}1 & 1 & 0\\ 0 & 0 & 0\end{Bmatrix}^2$$

$$= \frac{2}{3}\,\Delta\mathcal{E}_{np-is}\,\left|\langle r\rangle_{is}^{np}\right|^2. \tag{12}$$

The quadrupole OS ($k = 2$) can be written as

$$f_{nd-is}^{(2)} = 2\,\Delta\mathcal{E}_{nd-is}\left|\langle r^2\rangle_{is}^{nd}\right|^2\begin{Bmatrix}2 & 2 & 0\\ 0 & 0 & 0\end{Bmatrix}^2$$
$$= \frac{2}{5}\,\Delta\mathcal{E}_{nd-is}\,\left|\langle r^2\rangle_{is}^{nd}\right|^2. \tag{13}$$

Similarly, for the octupole OS ($k = 3$), the expression becomes

$$f_{nf-is}^{(3)} = 2\,\Delta\mathcal{E}_{nf-is}\left|\langle r^3\rangle_{is}^{nf}\right|^2\begin{Bmatrix}3 & 3 & 0\\ 0 & 0 & 0\end{Bmatrix}^2$$
$$= \frac{2}{7}\,\Delta\mathcal{E}_{nf-is}\,\left|\langle r^3\rangle_{is}^{nf}\right|^2. \tag{14}$$

And for the hexadecapole OS ($k = 4$), one gets

$$f_{ng-is}^{(4)} = 2\,\mathcal{E}_{ng-is}\left|\langle r^4\rangle_{is}^{ng}\right|^2\begin{Bmatrix}4 & 4 & 0\\ 0 & 0 & 0\end{Bmatrix}^2 \quad = \frac{2}{9}\,\Delta\mathcal{E}_{ng-is}\,\left|\langle r^4\rangle_{is}^{ng}\right|^2. \tag{15}$$

The analytical closed-form expressions for multipole oscillator strength ($k = 1 - 4$) for all possible transitions and polarizabilities in FHA are collected in Appendix A. It is important to mention that a multipole OS sum rule exists as follows:

$$S^{(k)} = \sum_m f^{(k)} = k\langle\psi_i|r^{(2k-2)}|\psi_i\rangle, \tag{16}$$

where the summation includes all the bound states.

C. Shannon entropy

Shannon entropy is a functional of the density. It provides the arithmetic mean of uncertainty [70–72]. In r and p spaces it can be expressed as

$$S_r = -\int_{R^3}\rho(r)\ln\rho(r)r^2dr,$$
$$S_p = -\int_{R^3}\Pi(p)\ln\Pi(p)p^2dp,$$
$$S_{\theta,\phi} = -\int\chi(\theta)\ln\chi(\theta)\sin\,\theta d\theta, \tag{17}$$
$$\chi(\theta) = |\Theta(\theta)|^2,$$
$$S_t = S_r + S_p + 2S_{\theta,\phi} \geqslant 3(1+\ln\pi),$$

where $\rho(r)$ and $\Pi(p)$ are the normalized position- and momentum-space densities, respectively. Barring a few cases, S_r and S_p have been evaluated numerically employing Eq. (17). In the present work, we employ S_r to determine the *critical screening constant* in WCP and ECSCP. In recent years, Shannon entropy has been investigated for confined H atoms [72–76].

D. Plasma characteristics

Plasma is a statistical system of mobile charged particles which interact with each other through electromagnetic forces. Here, the coupling occurs between quantum states and plasma density. Now we briefly discuss the characteristics of various H-atom plasmas.

In a hot plasma, the collective plasma-screening effect on a H atom is normally mapped by using a Debye-Hückel potential of the form [5]

$$V_1(r) = \begin{cases}-\frac{Z}{r}e^{-\lambda_1 r} & r \leqslant r_c,\\ 0 & r > r_c.\end{cases} \tag{18}$$

In this form of potential, the probability of finding plasma particles inside the Debye sphere is negligible. In addition to the screening effect, here, it is assumed that the charge cloud is confined in the spherical enclosure. This situation provides an alternate boundary condition for such systems. However, at $r_c \to \infty$ this restriction vanishes. The Debye radius ($D = \frac{1}{\lambda_1}$) plays an important role in WCP. For example, (i) at a fixed n_e, $D \propto \sqrt{T_e}$, and (ii) at a certain T_e, $D \propto \frac{1}{\sqrt{n_e}}$. Most importantly, at a constant D, $n_e \propto T_e$. This result means that, to keep λ_1 or D fixed, with a rise in T_e, n_e increases. Further, with an increase in n_e, the plasma-tail effect declines. Conversely, with a rise in T_e, it is enhanced. But, here, incorporation of radial confinement indirectly controls the tail effect. It is important to mention that, the plasma-tail effect arises due to the presence of asymptotic part of the plasma potential. With an increase in T_e, the ions get diffused, leading to an enhancement of this effect. When r_c is large, then T_e predominates over n_e. On the other hand, in the low-r_c region, the effect of n_e prevails. Therefore, in this work, we have probed WCP in two different ways: (i) with the variation of r_c at a fixed λ_1 and (ii) with the effect of λ_1 at a certain r_c. Figure 1(a) shows that an enhancement in λ_1 leads to a growth in plasma electron density surrounding the positive ion.

With an increase in plasma density, the multiparticle cooperative interaction is enhanced. Thus, D becomes comparable to the de Broglie wavelength, and hence, the quantum effect appears [77]. In this context, the Debye-Hückel model becomes inappropriate to explain the plasma properties. In ECSCP, λ_2 is connected to plasma frequency as $\lambda_2 \propto \sqrt{\omega_{pe}}$. It has the form

$$V_2(r) = \begin{cases}-\frac{Z}{r}e^{-\lambda_2 r}\,\cos(\lambda_2 r) & r \leqslant r_c,\\ 0 & r > r_c.\end{cases} \tag{19}$$

Due to the incorporation of the cosine term, ECSCP exhibits a stronger screening effect than WCP. There occurs a maximum at $r_{\max} = \frac{\pi}{2\lambda_2}$. The temperature connection to λ_2 is not known. However, like WCP, here also, r_c plays the same role: with an increase in r_c, the temperature effect is enhanced. Figure 1(b) indicates that, with a rise in λ_2, the position of the maximum gets left shifted and hence the plasma density increases. Like WCP, here, too, the effects of both λ_2 and r_c are explored. At $\lambda = 0$, both WCP and ECSCP modify to FHA-like systems.

In the case of SP, the ion experiences a spherically symmetric environment within a radius R, commonly known as the Wigner-Seitz radius. Beyond R, the effect of the potential vanishes. Hence, the potential is expressed as

$$V_3(r) = \begin{cases}-\frac{Z}{r} + \frac{Z-N_e}{2R}\left[3 - \left(\frac{r}{R}\right)^2\right], & \\ 0 \qquad r > r_c = R.\end{cases} \tag{20}$$

With a decrease in R, n_e increases and vice versa. T_e does not appear directly in this case. However, it is implicit that

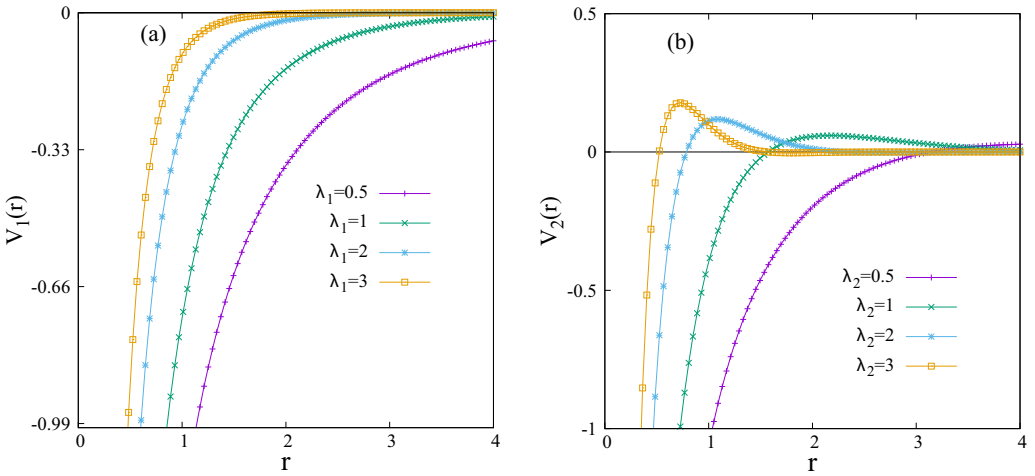

FIG. 1. Plots of (a) $V_1(r)$, Eq. (18), and (b) $V_2(r)$, Eq. (19), against r (in a.u.), at selected λ values, namely, 0.5, 1, 2, 3, keeping $Z = 2$. For details, see the text.

the change in R exerts the effect of T_e. At $r_c \to \infty$, Eq. (20) reduces to a FHA. It is necessary to mention that in SP the $Z \geqslant 2$ condition needs to be obeyed.

E. Scaling transformation

In the case of plasma potentials, the scaling concept was implied previously in Refs. [8,35,39,61]. This work employs two independent scaling ideas and attempts to derive a single equation connecting the original and scaled Hamiltonians. Thus, starting from an arbitrary set of Z and β, one can easily estimate a given desired property for a series of Z and β, connected by the scaling relation. To proceed further, one can write Eq. (3) as follows:

$$-\frac{\hbar^2}{2m}\frac{d^2}{dr^2}\psi_{n,\ell}(r)+V_c(Z;\beta;r)\psi_{n,\ell}(r)+V_0\theta(r-r_c)\psi_{n,\ell}(r) = \mathcal{E}_{n,\ell}\ \psi_{n,\ell}(r),$$
$$\theta(r-r_c)=0 \quad \text{for} \quad r \leqslant r_c, \qquad \theta(r-r_c)=1 \quad \text{for} \quad r > r_c. \tag{21}$$

Here, $V_c(Z,\beta,r)$ is the potential that describes a H atom under the influence of the plasma environment, $\theta(r-r_c)$ is the Heaviside theta function, and V_0 is taken to be an infinitely large positive constant. The use of atomic units, $\hbar = m = 1$, transforms Eq. (21) as

$$-\frac{1}{2}\frac{d^2}{dr^2}\ \psi_{n,\ell}(r)+V_c(Z;\beta;r)\ \psi_{n,\ell}(r)+V_0\theta(r-r_c)\ \psi_{n,\ell}(r) = \mathcal{E}_{n,\ell}\ \psi_{n,\ell}(r). \tag{22}$$

For H-isoelectronic series, it is interesting to probe the impact of Z as well as β on the properties of a given system. Now analytical relations among $\langle\hat{T}^n\rangle$, $\langle\hat{V}^n\rangle$, $\langle\hat{T}\hat{V}\rangle$, $f_{ni}^{(k)}$, and $\alpha_{ni}^{(k)}$ with Z and β will be established by employing two independent, parallel scaling transformations.

(1) In the first case, we apply a transformation ($r = Zr_1$). The Hamiltonian can then be modified in the following form:

$$H(Z;\beta;r_c;r) \to H\left(1;\frac{\beta}{Z};Zr_c;r_1\right). \tag{23}$$

Thus, the Z-containing part of the potential becomes independent of it.

This substitution transforms the Hamiltonian in Eq. (21) into following form:

$$-\frac{1}{2}\nabla_1^2\psi_{n,\ell}(r_1)+V_c\left(1,\frac{\beta}{Z},r_1\right)\psi_{n,\ell}(r_1) + Z^2V_0\theta(r_1-Zr_c)\psi_{n,\ell}(r_1) = Z^2\ \mathcal{E}_{n,\ell}\ \psi_{n,\ell}(r_1). \tag{24}$$

The eigenfunctions and eigenvalues of the initial and modified Hamiltonians are connected as

$$\mathcal{E}_{n,\ell}[1;Z;\beta;r_c] = Z^2\mathcal{E}_{n,\ell}\left[1;1;\frac{\beta}{Z};Zr_c\right],$$
$$\psi_{n,\ell}(1;Z;\beta;r_c;r) = \frac{1}{Z^{\frac{3}{2}}}\psi_{n,\ell}\left(1;1;\frac{\beta}{Z};Zr_c;r_1\right). \tag{25}$$

Then $\langle\hat{T}^n\rangle$, $\langle\hat{V}^n\rangle$, $\langle\hat{T}\hat{V}\rangle$, and Z are found to be related as

$$\langle\hat{V}^n\rangle[1;Z;\beta;r_c] = Z^{2n}\ \langle\hat{V}^n\rangle\left[1;1;\frac{\beta}{Z};Zr_c\right],$$
$$\langle\hat{T}^n\rangle[1;Z;\beta;r_c] = Z^{2n}\ \langle\hat{T}^n\rangle\left[1;1;\frac{\beta}{Z};Zr_c\right],$$
$$\langle\hat{T}\hat{V}\rangle[1;Z;\beta;r_c] = Z^{4}\ \langle\hat{T}\hat{V}\rangle\left[1;1;\frac{\beta}{Z};Zr_c\right],$$
$$\langle\hat{V}\hat{T}\rangle[1;Z;\beta;r_c] = Z^{4}\ \langle\hat{V}\hat{T}\rangle\left[1;1;\frac{\beta}{Z};Zr_c\right]. \tag{26}$$

The multipole OS now takes the form

$$f_{ni}^{(k)}[1;Z;\beta;r_c] = \frac{f_{ni}^{(k)}\left[1;1;\frac{\beta}{Z};Zr_c\right]}{Z^{2(k-1)}}. \tag{27}$$

This equation suggests that the dipole ($k = 1$) OS is independent of this scaling transformation. However, quadrupole ($k = 2$), octupole ($k = 3$), and hexadecapole ($k = 4$) OSs depend on Z. Now, some simple mathematical manipulation provides the modified expression of $\alpha_i^{(k)}$(bound) as follows:

$$\alpha_i^{(k)}(\text{bound})[1;Z;\beta;r_c] = \frac{\alpha_i^{(k)}(\text{bound})\left[1;1;\frac{\beta}{Z};Zr_c\right]}{Z^{2k+2}}. \tag{28}$$

(2) Another transformation ($r = \frac{r_2}{\beta}$) can be applied to alter the same Hamiltonian as

$$H(Z;\beta;r_c;r) \to H\left(\frac{Z}{\beta};1;\beta r_c;r_2\right). \tag{29}$$

Now the potential is mapped such that the β-containing part becomes free of it.

The substitution of $r = \frac{r_2}{\beta}$ transforms the Hamiltonian in Eq. (21) into the form

$$-\frac{1}{2}\nabla^2\psi_{n,\ell}(r_2) + V_c\left(\frac{Z}{\beta};1;r_2\right)\psi_{n,\ell}(r_2) + \frac{1}{\beta^2}V_0\theta(r_2-\beta r_c)\psi_{n,\ell}(r_2) = \left(\frac{\mathcal{E}_{n,\ell}}{\beta^2}\right)\psi_{n,\ell}(r_2). \tag{30}$$

The eigenfunctions and eigenvalues of the initial and modified Hamiltonians are related as

$$\mathcal{E}_{n,\ell}[1;Z;\beta;r_c] = \beta^2,\ \ \mathcal{E}_{n,\ell}\left[1;\frac{Z}{\beta};1;\beta r_c\right],$$
$$\psi_{n,\ell}(1;Z;\beta;r_c;r) = \beta^{\frac{3}{2}},\ \psi_{n,\ell}\left(1;\frac{Z}{\beta};1;\beta r_c;r_2\right). \tag{31}$$

Then $\langle\hat{T}^n\rangle$, $\langle\hat{V}^n\rangle$, $\langle\hat{T}\hat{V}\rangle$, and β are connected as

$$\langle\hat{V}^n\rangle[1;Z;\beta;r_c] = \beta^{2n}\ \langle\hat{V}^n\rangle\left[1;\frac{Z}{\beta};1;\beta r_c\right],$$
$$\langle\hat{T}^n\rangle[1;Z;\beta;r_c] = \beta^{2n}\ \langle\hat{T}^2\rangle\left[1;\frac{Z}{\beta};1;\beta r_c\right],$$
$$\langle\hat{T}\hat{V}\rangle[1;Z;\beta;r_c] = \beta^{4}\ \langle\hat{T}\hat{V}\rangle\left[1;\frac{Z}{\beta};1;\beta r_c\right],$$
$$\langle\hat{V}\hat{T}\rangle[1;Z;\beta;r_c] = \beta^{4}\ \langle\hat{V}\hat{T}\rangle\left[1;\frac{Z}{\beta};1;\beta r_c\right]. \tag{32}$$

Now, using Eq. (26) in Eq. (9), the multipole OS can have the generalized form

$$f_{ni}^{(k)}[1;Z;\beta;r_c] = \left(\frac{f_{ni}^{(k)}\left[1;\frac{Z}{\beta};1;\beta r_c\right]}{\beta^{(2k-2)}}\right). \tag{33}$$

This implies that the dipole OS is invariant under this scaling transformation. However, higher-order ($k > 1$) OSs depend on β. Again, some straightforward mathematical manipulation gives the modified expression of $\alpha_i^{(k)}$(bound) as

$$\alpha_i^{(k)}(\text{bound})[1;Z;\beta;r_c] = \left(\frac{\alpha_i^{(k)}(\text{bound})\left[1;\frac{Z}{\beta};1;\beta r_c\right]}{\beta^{2(k+1)}}\right). \tag{34}$$

Thus, we have successfully converted the initial Hamiltonian, Eq. (3), into two independent scaled Hamiltonians, viz., Eqs. (24) and (30). Now, the connecting relations are

$$\mathcal{E}_{n,\ell}[1;Z;\beta;r_c] = Z^2\mathcal{E}_{n,\ell}\left[1;1;\frac{\beta}{Z};Zr_c\right] = \beta^2\mathcal{E}_{n,\ell}\left[1;\frac{Z}{\beta};1;\beta r_c\right]. \tag{35}$$

Some reorganization leads to the following:

$$\frac{\mathcal{E}_{n,\ell}\left[1;1;\frac{\beta}{Z};Zr_c\right]}{\mathcal{E}_{n,\ell}\left[1;\frac{Z}{\beta};1;\beta r_c\right]} = \left(\frac{\beta}{Z}\right)^2. \tag{36}$$

The expectation values then satisfy the following relations:

$$\langle\hat{V}^n\rangle[1;Z;\beta;r_c] = Z^{2n}\langle\hat{V}^n\rangle\left[1;1;\frac{\beta}{Z};Zr_c\right] = \beta^{2n}\langle\hat{V}^n\rangle\left[1;\frac{Z}{\beta};1;\beta r_c\right]. \tag{37}$$

A slight rearrangement of the above equation leads to

$$\frac{\langle\hat{V}^n\rangle\left[1;1;\frac{\beta}{Z};Zr_c\right]}{\langle\hat{V}^n\rangle\left[1;\frac{Z}{\beta};1;\beta r_c\right]} = \left(\frac{\beta}{Z}\right)^{2n}. \tag{38}$$

In the case of kinetic energy, one gets

$$\langle\hat{T}^n\rangle[1;Z;\beta;r_c] = Z^{2n}\langle\hat{T}^n\rangle\left[1;1;\frac{\beta}{Z};Zr_c\right] = \beta^{2n}\langle\hat{T}^n\rangle\left[1;\frac{Z}{\beta};1;\beta r_c\right], \tag{39}$$

which, upon rearrangement, gives

$$\frac{\langle\hat{T}^n\rangle\left[1;1;\frac{\beta}{Z};Zr_c\right]}{\langle\hat{T}^n\rangle\left[1;\frac{Z}{\beta};1;\beta r_c\right]} = \left(\frac{\beta}{Z}\right)^{2n}. \tag{40}$$

The multipole OS accordingly becomes

$$f_{ni}^{(k)}[1;Z;\beta;r_c] = \frac{f_{ni}^{(k)}\left[1;1;\frac{\beta}{Z};Zr_c\right]}{Z^{2(k-1)}} = \frac{f_{ni}^{(k)}\left[1;\frac{Z}{\beta};1;\beta r_c\right]}{\beta^{2(k-1)}}, \tag{41}$$

which can be recast to yield

$$\frac{f_{ni}^{(k)}\left[1;1;\frac{\beta}{Z};Zr_c\right]}{f_{ni}^{(k)}\left[1;\frac{Z}{\beta};1;\beta r_c\right]} = \left(\frac{Z}{\beta}\right)^{2(k-1)}. \tag{42}$$

Finally, the polarizabilities are connected as

$$\alpha_i^{(k)}(\text{bound})[1;Z;\beta;r_c] = \frac{\alpha_i^{(k)}(\text{bound})\left[1;1;\frac{\beta}{Z};Zr_c\right]}{Z^{2(k+1)}} = \frac{\alpha_i^{(k)}(\text{bound})\left[1;\frac{Z}{\beta};1;\beta r_c\right]}{\beta^{2(k+1)}}. \tag{43}$$

This can be written in the following form:

$$\frac{\alpha_i^{(k)}(\text{bound})\left[1;1;\frac{\beta}{Z};Zr_c\right]}{\alpha_i^{(k)}(\text{bound})\left[1;\frac{Z}{\beta};1;\beta r_c\right]} = \left(\frac{Z}{\beta}\right)^{2(k+1)}. \tag{44}$$

The foregoing discussion thus shows that a connection formula, as follows, can be derived among three Hamiltonians, corresponding to the SE in Eqs. (3), (24), and (30):

$$H\left(1;1;\frac{\beta}{Z};Zr_c;r_1\right) \leftrightarrow H(1;Z;\beta;r_c;r) \leftrightarrow H\left(1;\frac{Z}{\beta};1;\beta r_c;r_2\right). \tag{45}$$

The above equation signifies that, performing the calculation at a particular (Z,β) pair, one can evaluate the properties of the other pair of (Z,β) (connected by scaling) without solving

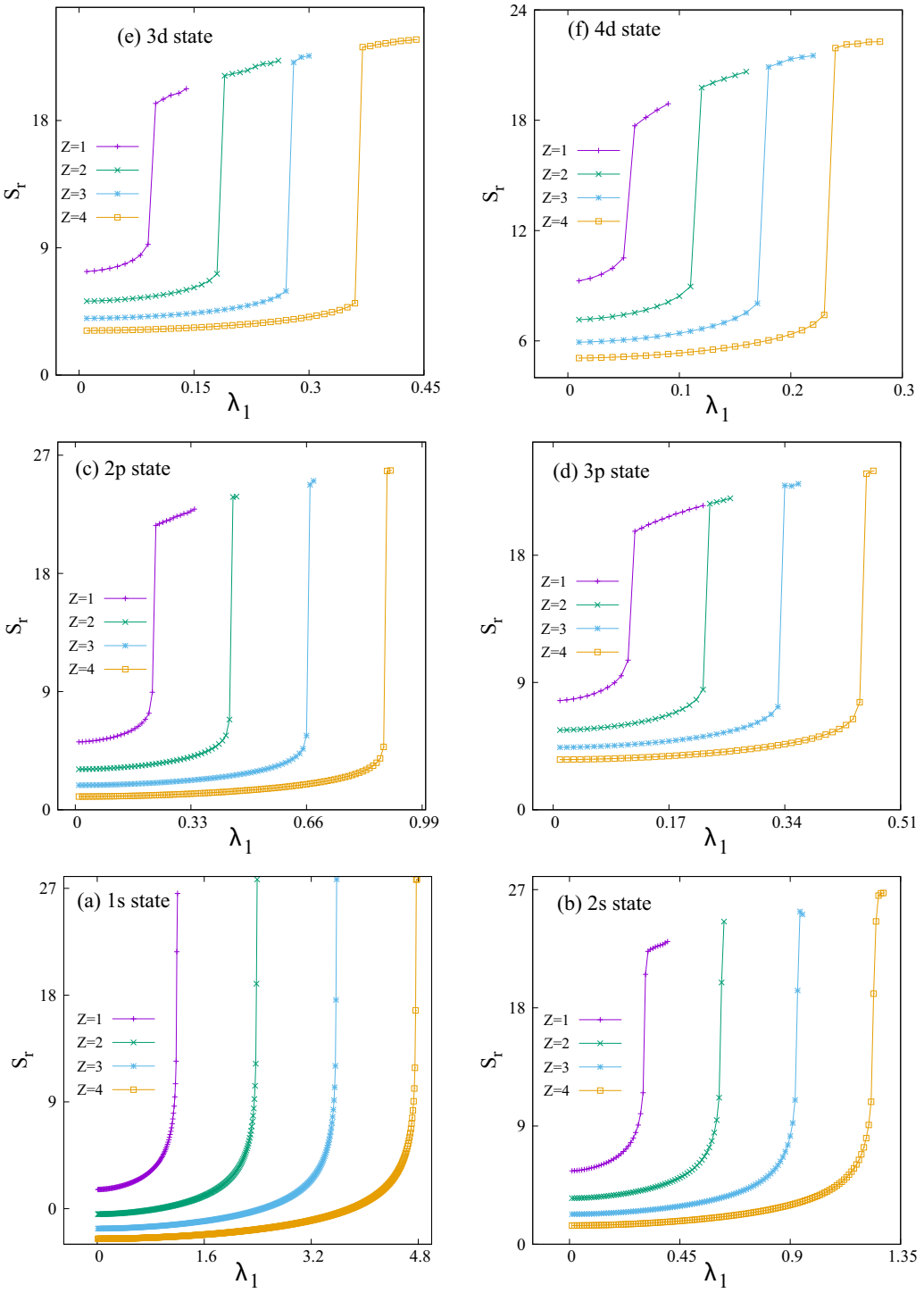

FIG. 2. Plot of S_r as a function of λ_1 (in a.u.) in WCP for (a) $1s$, (b) $2s$, (c) $2p$, (d) $3p$, (e) $3d$, and (f) $4d$ states at four selected values of Z, namely, 1, 2, 3, 4. See the text for details.

the SE. These are derived for any two-parameter potentials. These relations are applicable in all three potentials used for the plasma characteristics in Sec. II C. In WCP, ECSCP, and SP, β becomes $\lambda_1, \lambda_2, \sigma = (\frac{Z-Ne}{2R^3})^{\frac{1}{4}}$, respectively. Some representative numerical results ($\mathcal{E}_{n,\ell}$, $f^{(1)}_{ns\to 2p}$, $\alpha^{(1)}_{ns}$) for these three Hamiltonians (connecting WCP, ECSCP, SP) are provided in Table V in Appendix B.

III. RESULTS AND DISCUSSION

In this section, first, we discuss the critical screening constant in WCP and ECSCP. Then, the usefulness and efficacy of VT are verified for WCP, ECSCP, and SP successively. Next, we report the multipole OS and polarizabilities for all three potentials. Pilot calculations are done for $1s$ and $2s$ states, choosing $Z = 2$. Of course, employing the scaling

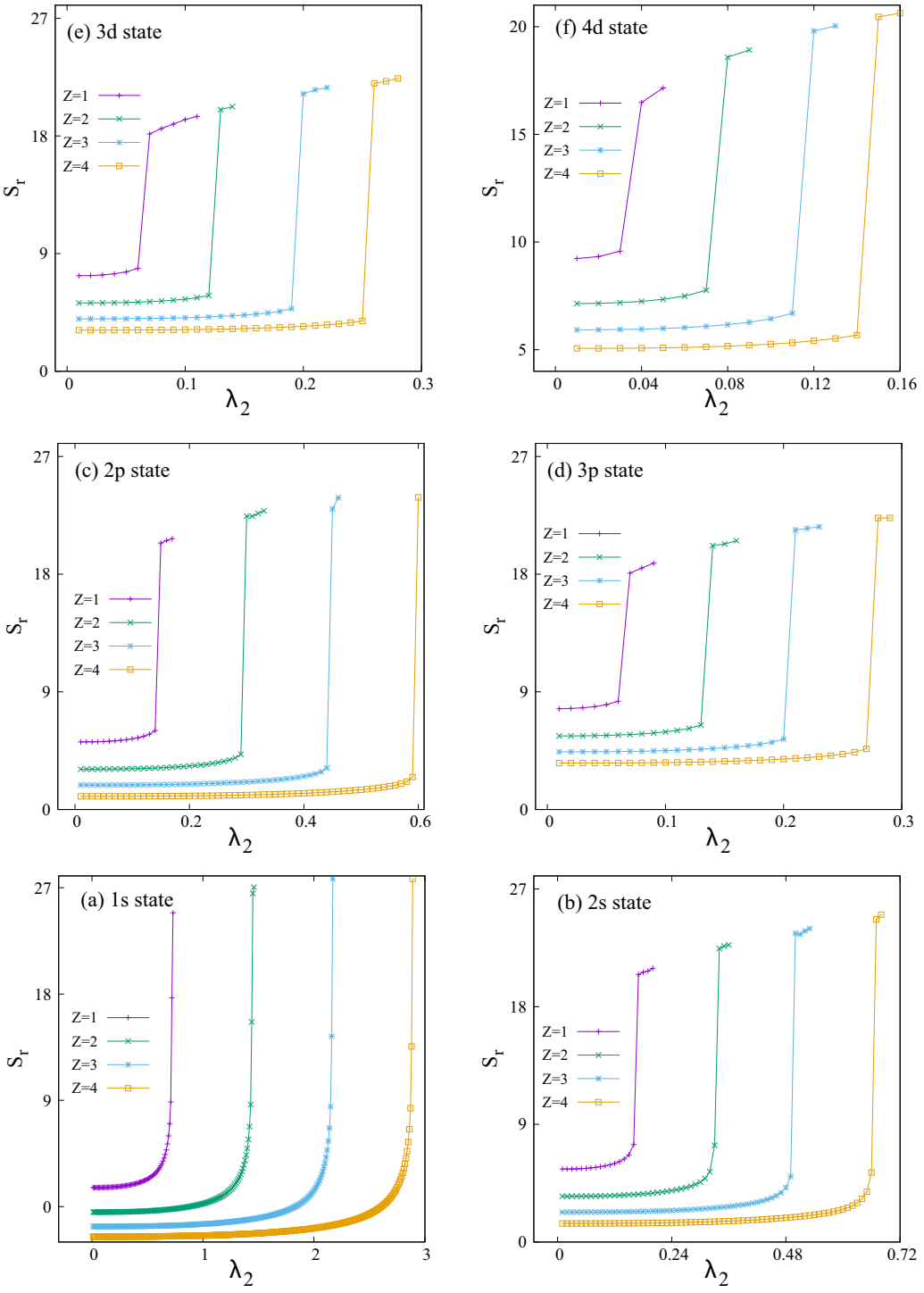

FIG. 3. Plot of S_r as a function of λ_2 (in a.u.) in ECSCP for (a) 1s, (b) 2s, (c) 2p, (d) 3p, (e) 3d, and (f) 4d states at four selected values of Z, namely, 1, 2, 3, 4. See the text for details.

relations of Eqs. (25)–(28), one can easily extract the result for other Z values. For ease of convenience, we have adopted the following notation. Use of λ in the text implies *both* λ_1 and λ_2, while explicit use of λ_1 or λ_2 refers to only WCP and ECSCP.

A. Critical screening constant in WCP and ECSCP

In WCP and ECSCP (at $r_c \to \infty$), the number of bound states reduces with the rise in the screening parameter λ. Several attempts were made to estimate the characteristic value of λ at which a particular state vanishes. Accurate numerical

TABLE I. $\lambda^{(c)}_{n,\ell}$ for H-like ion for $1s$, $2s$, $2p$, $3p$, $3d$, $4d$ states in WCP and ECSCP. See the text for details.

WCP				ECSCP			
Z	State	$\lambda^{(c)}_{n,\ell}$	$\mathcal{E}_{n,\ell}$	Z	State	$\lambda^{(c)}_{n,\ell}$	$\mathcal{E}_{n,\ell}$
1	$1s$	1.1856[a,b]	−0.00000656	1	$1s$	0.7196[c]	−0.00000531
2		2.3712	−0.00002650	2	$1s$	1.4384	−0.00002124
3		3.5573	−0.00005964	3	$1s$	2.1576	−0.00004779
4		4.7410	−0.00010265	4	$1s$	2.8756	−0.00008496
1	$2s$	0.3063[b]	−0.00000995	1	$2s$	0.1664[c]	−0.00000552
2		0.6124	−0.00003960	2	$2s$	0.3328	−0.00002206
3		0.9195	−0.00008970	3	$2s$	0.4992	−0.00004965
4		1.2254	−0.00015925	4	$2s$	0.6656	−0.00008826
1	$2p$	0.2206[b]	−0.00000723	1	$2p$	0.1482[c]	−0.00000234
2		0.4404	−0.00002860	2	$2p$	0.2964	−0.00000937
3		0.6606	−0.00006341	3	$2p$	0.4446	−0.00002109
4		0.8821	−0.00011341	4	$2p$	0.5928	−0.00003749
1	$3p$	0.1126[b]	−0.00000701	1	$3p$	0.0687[c]	−0.00000488
2		0.2254	−0.00002854	2	$3p$	0.1374	−0.00001950
3		0.3381	−0.00006371	3	$3p$	0.2061	−0.00004388
4		0.4504	−0.00011208	4	$3p$	0.2748	−0.00007801
1	$3d$	0.0914[b]	−0.00000878	1	$3d$	0.0635[c]	−0.00001937
2		0.1826	−0.00003614	2	$3d$	0.1271	−0.00007787
3		0.2739	−0.00008030	3	$3d$	0.1907	−0.00017251
4		0.3653	−0.00012718	4	$3d$	0.2542	−0.00031150
1	$4d$	0.0581[b]	−0.00000974	1	$4d$	0.0374[c]	−0.00000260
2		0.1161	−0.00003951	2	$4d$	0.0748	−0.00001041
3		0.1741	−0.00008364	3	$4d$	0.1122	−0.00002342
4		0.2321	−0.00016672	4	$4d$	0.1496	−0.00004164

[a]Literature result for $\lambda^{(c)}_{1,0}$ [8]: 1.190612421.
[b]Literature results for $\lambda^{(c)}_{n,\ell}$ [55,56]: (a) $\lambda^{(c)}_{1s} = 1.190610$, (b) $\lambda^{(c)}_{2s} = 0.310199$, (c) $\lambda^{(c)}_{2p} = 0.220216$, (d) $\lambda^{(c)}_{3p} = 0.112710$, (e) $\lambda^{(c)}_{3d} = 0.091345$, and (f) $\lambda^{(c)}_{4d} = 0.058105$.
[c]Literature results for $\lambda^{(c)}_{n,\ell}$ [44,55,56]: (a) $\lambda^{(c)}_{1s} = 0.720524$, (b) $\lambda^{(c)}_{2s} = 0.166617$, (c) $\lambda^{(c)}_{2p} = 0.148205$, (d) $\lambda^{(c)}_{3p} = 0.068712$, (e) $\lambda^{(c)}_{3d} = 0.063581$, and (f) $\lambda^{(c)}_{4d} = 0.037405$.

results are available up to $6h$ states of a H atom in WCP [40,56] and ECSCP [44,55,56]. Further, in Ref. [39], the relation between this critical constant $\lambda^{(c)}_{n,\ell}(Z)$ and Z was derived for the ground state in WCP. These values are determined by applying the sign-change argument in energy. Instead of that, here, we have applied a simple density-based technique to ascertain these points in WCP and ECSCP. For that purpose, S_r [given in Eq. (17)] has been employed. Based on this study, a uniform relation between these two quantities [$\lambda^{(c)}_{n,\ell}(Z)$ and Z] is offered. It may be applied to an arbitrary state. Furthermore, a similar relation is also obtained by employing the scaling concept and some empirical idea (see below).

The calculated S_r as a function of λ_1 for the first two states of each $\ell = 0$–2 are displayed in Fig. 2. Figures 2(a)–2(f) represent $1s$, $2s$, $2p$, $3p$, $3d$, $4d$ states, respectively. In each of these panels one can see equispaced curves corresponding to $Z = 1$–4. At a fixed Z, in each of these states a sudden jump in S_r occurs at a characteristics λ_1. Therefore, S_r can indicate the critical point at which a particular state vanishes. Further, at a certain Z, S_r increases with λ_1. It means that with a decrease in D the confinement effect weakens. Conversely, with a rise in T_e this effect predominates. Analogous plots are supplied in Figs. 3(a)–3(f) for ECSCP, involving the same six states as in Fig. 2. The qualitative behaviors of S_r in WCP and ECSCP remain quite similar. In each state, a stiff increase in S_r occurs at a certain λ_2 value. Interestingly, with a rise in Z, this S_r vs λ_2 curve gets right shifted. Further, these curves are placed equidistant from each other. From the above, it is clear that S_r can be used to determine the critical screening constant in a given potential. Note that, in both potentials, for a given state, the ratio of the screening constant and Z is a constant because the four curves remain evenly separated. Depending upon these outcomes, one can derive an empirical relation between $\lambda_{n,\ell}$ and Z.

Both in WCP and ECSCP, the Hamiltonian in the *free condition* is scaled as

$$H(Z;\lambda) \to H\left(1;\frac{\lambda}{Z}\right). \tag{46}$$

Similarly, energy in a definite (n, ℓ) state is scaled as

$$\mathcal{E}_{n,\ell}(Z;\lambda) = Z^2\mathcal{E}_{n,\ell}\left(1;\frac{\lambda}{Z}\right). \tag{47}$$

Therefore, one can easily write the following relations for both the WCP and ECSCP cases:

$$\frac{\lambda^{(c)}_{n,\ell}}{Z} \approx \lambda^{(c)}_{n,\ell}(Z=1),$$
$$\lambda^{(c)}_{n,\ell}(Z) \approx Z\,\lambda^{(c)}_{n,\ell}(Z=1). \tag{48}$$

TABLE II. $\mathcal{E}_{n,\ell}$, $(\Delta\hat{V}_{n,\ell})^2$, $(\Delta\hat{T}_{n,\ell})^2$, $\langle\hat{T}\rangle_{n,\ell}\langle\hat{V}\rangle_{n,\ell} - \langle\hat{T}\hat{V}\rangle_{n,\ell}$, and $\langle\hat{T}\rangle_{n,\ell}\langle\hat{V}\rangle_{n,\ell} - \langle\hat{V}\hat{T}\rangle_{n,\ell}$ of the $1s, 2s$ states in WCP, ECSCP, and SP, choosing $Z = 2$, at six different sets of (λ_1, r_c), (λ_2, r_c), and r_c, respectively.

		WCP					
State	Quantity	$\lambda_1 = 0.1$, $r_c = 0.1$	$\lambda_1 = 0.1$, $r_c = 0.5$	$\lambda_1 = 0.5$, $r_c = 0.5$	$\lambda_1 = 1$, $r_c = 1$	$\lambda_1 = 1.5$, $r_c = 5$	$\lambda_1 = 0.45$, $r_c = \infty$
	$\mathcal{E}_{1,0}$	444.47894213	9.69364280	10.43995746	1.13262338	−0.22737500	−1.23411551
	$(\Delta\hat{V}_{1,0})^2$	1285.99378348	71.83641411	71.53062216	26.32910366	8.20218577	15.00733998
$1s$	$(\Delta\hat{T}_{1,0})^2$	1285.99378348	71.83641411	71.53062216	26.32910366	8.20218577	15.00733998
	$\langle\hat{T}\rangle_{1,0}\langle\hat{V}\rangle_{1,0} - \langle\hat{T}\hat{V}\rangle_{1,0}$	1285.99378355	71.83641411	71.53062216	26.32910366	8.20218577	15.00733998
	$\langle\hat{T}\rangle_{1,0}\langle\hat{V}\rangle_{1,0} - \langle\hat{V}\hat{T}\rangle_{1,0}$	1285.99378355	71.83641411	71.53062216	26.32910366	8.20218577	15.00733998
	$\mathcal{E}_{2,0}$	1911.60619014	66.47853464	67.22135372	14.89326554	0.38477218	−0.02806813
	$(\Delta\hat{V}_{2,0})^2$	3787.39749470	180.91460373	180.32580299	53.43300740	3.14499616	1.08218497
$2s$	$(\Delta\hat{T}_{2,0})^2$	3787.39749470	180.91460373	180.32580299	53.43300740	3.14499616	1.08218497
	$\langle\hat{T}\rangle_{2,0}\langle\hat{V}\rangle_{2,0} - \langle\hat{T}\hat{V}\rangle_{2,0}$	3787.39749467	180.91460373	180.32580300	53.43300740	3.14499616	1.08218497
	$\langle\hat{T}\rangle_{2,0}\langle\hat{V}\rangle_{2,0} - \langle\hat{V}\hat{T}\rangle_{2,0}$	3787.39749467	180.91460373	180.32580300	53.43300740	3.14499616	1.08218497
		ECSCP					
State	Quantity	$\lambda_2 = 0.1$, $r_c = 0.1$	$\lambda_2 = 0.1$, $r_c = 0.5$	$\lambda_2 = 0.5$, $r_c = 0.5$	$\lambda_2 = 1$, $r_c = 1$	$\lambda_2 = 1.5$, $r_c = 5$	$\lambda_2 = 0.25$, $r_c = \infty$
	$\mathcal{E}_{1,0}$	444.47943354	9.69592190	10.49107011	1.39032540	0.07291645	−1.50671442
	$(\Delta\hat{V}_{1,0})^2$	1286.00324892	71.84954944	71.80723304	27.20420371	4.95684246	15.91293469
$1s$	$(\Delta\hat{T}_{1,0})^2$	1286.00324892	71.84954944	71.80723304	27.20420371	4.95684246	15.91293469
	$\langle\hat{T}\rangle_{1,0}\langle\hat{V}\rangle_{1,0} - \langle\hat{T}\hat{V}\rangle_{1,0}$	1286.00324885	71.84954944	71.80723304	27.20420371	4.95684246	15.91293469
	$\langle\hat{T}\rangle_{1,0}\langle\hat{V}\rangle_{1,0} - \langle\hat{V}\hat{T}\rangle_{1,0}$	1286.00324885	71.84954944	71.80723304	27.20420371	4.95684246	15.91293469
	$\mathcal{E}_{2,0}$	1911.60668730	66.48097112	67.27483408	15.15621209	0.49330671	−0.07314818
	$(\Delta\hat{V}_{2,0})^2$	3787.42042508	180.93992940	180.85424331	54.56130508	4.89088914	2.26239187
$2s$	$(\Delta\hat{T}_{2,0})^2$	3787.42042508	180.93992940	180.85424331	54.56130508	4.89088914	2.26239187
	$\langle\hat{T}\rangle_{2,0}\langle\hat{V}\rangle_{2,0} - \langle\hat{T}\hat{V}\rangle_{2,0}$	3787.42042492	180.93992940	180.85424331	54.56130508	4.89088914	2.26239187
	$\langle\hat{T}\rangle_{2,0}\langle\hat{V}\rangle_{2,0} - \langle\hat{V}\hat{T}\rangle_{2,0}$	3787.42042492	180.93992940	180.85424331	54.56130508	4.89088914	2.26239187
		SP					
State	Quantity	$r_c = 0.1$	$r_c = 0.5$	$r_c = 1$	$r_c = 2$	$r_c = 5$	$r_c = 10$
	$\mathcal{E}_{1,0}$	471.50566905	14.98747298	2.27917566	−0.50537037	−1.40602867	−1.70075051
	$(\Delta\hat{V}_{1,0})^2$	1207.82025521	67.49838821	26.33780873	16.31778893	15.91807847	15.98870703
$1s$	$(\Delta\hat{T}_{1,0})^2$	1207.82025521	67.49838821	26.33780873	16.31778893	15.91807847	15.98870703
	$\langle T\rangle_{1,0}\langle\hat{V}\rangle_{1,0} - \langle\hat{T}\hat{V}\rangle_{1,0}$	1207.82025512	67.49838821	26.33780873	16.31778893	15.91807847	15.98870703
	$\langle T\rangle_{1,0}\langle\hat{V}\rangle_{1,0} - \langle\hat{V}\hat{T}\rangle_{1,0}$	1207.82025512	67.49838821	26.33780873	16.31778893	15.91807847	15.98870703
	$\mathcal{E}_{2,0}$	1938.19369550	71.63098684	15.97749590	3.00469070	0.09030651	−0.21064190
	$(\Delta\hat{V}_{2,0})^2$	3589.04237047	172.06135205	53.23498447	18.29571481	3.69613370	2.88000313
$2s$	$(\Delta\hat{T}_{2,0})^2$	3589.04237047	172.06135205	53.23498447	18.29571481	3.69613370	2.88000313
	$\langle\hat{T}\rangle_{2,0}\langle\hat{V}\rangle_{2,0} - \langle\hat{T}\hat{V}\rangle_{2,0}$	3589.04237064	172.06135205	53.23498447	18.29571481	3.69613370	2.88000313
	$\langle\hat{T}\rangle_{2,0}\langle\hat{V}\rangle_{2,0} - \langle\hat{V}\hat{T}\rangle_{2,0}$	3589.04237064	172.06135205	53.23498447	18.29571481	3.69613370	2.88000313

The relation in Eq. (48) is in excellent agreement with those achieved by computing S_r in WCP and ECSCP. Representative numerical results are provided in Table I for $Z = 1$–4 involving the same six states as in Figs. 1 and 2 in WCP and ECSCP. These critical parameters are compared with available reference results (for $Z = 1$), which show very good matching in both WCP [55,56] and ECSCP [44,55,56]. However, to the best of our knowledge, no such data have been reported for $Z > 1$. The critical points from the sign-change argument also complement the outcomes achieved by employing the information-entropy concept. This shows that S_r may act as an efficient indicator for finding critical points and may be utilized in the future. As expected, the tabular results strongly recommend the proposition of Eq. (48) in both WCP and ECSCP. For the sake of completeness, $\lambda^{(c)}_{n,\ell}$ are computed for all the remaining states corresponding to $\ell = 5$ $(3s, 4s, 4p, 4f, 5s, 5p, 5d, 5f, 5g)$. They are reported in Table VI in Appendix C, along with the appropriate references.

B. Virial-like theorem

As mentioned in Sec. II A, the conventional VT is not satisfied in the confined condition. Recently [63], a virial-like expression was derived and successfully applied to a H atom trapped in various confined environments [63]. It was found that, in the end, the perturbing potential does not appear in the final expression. In this section, we probe this theorem in the context of WCP, ECSCP, and SP successively.

TABLE III. $f^{(1)}$ values for WCP and ECSCP (in free and confined conditions) and SP involving the $ns \to 2p$ and $ns \to 3p$ ($n = 1, 2$) transitions. See the text for details.

	Confined WCP						Free WCP	
Transition	λ_1	$r_c = 0.1$	$r_c = 0.5$	$r_c = 1$	$r_c = 2$	$r_c = 5$	λ_1	$r_c = \infty$
$1s \to 2p$	0.1	0.97072714	0.98455633	0.99105667	0.92744965	0.48674542	0.1	0.40181907
	0.5	0.97072657	0.98450970	0.99101296	0.93172951	0.42593118	0.2	0.36301391
	1	0.97072481	0.98437662	0.99088526	0.94270974	0.42487213	0.3	0.29859664
	2.2	0.97071618	0.98380464	0.99014361	0.97196847	0.84116523	0.4	0.19333749
$1s \to 3p$	0.1	0.02145207	0.00772756	0.00000194	0.04896547	0.30906124	0.01	0.07892729
	0.5	0.02145255	0.00776480	0.00000008	0.04498399	0.32619988	0.05	0.07536052
	1	0.02145402	0.00787227	0.00002302	0.03498548	0.07783255	0.1	0.06581437
	2.2	0.02146127	0.00834459	0.00047966	0.00951569	0.26193927	0.2	0.02982086
$2s \to 2p$	0.1	−0.59617944	−0.60825425	−0.61188356	−0.54000701	−0.06993817	0.1	0.01961263
	0.4	−0.59617891	−0.60820263	−0.61167657	−0.54121728	0.00417437	0.2	0.07522974
	0.5	−0.59617859	−0.60817302	−0.61156439	−0.54200502	0.03181610	0.3	0.17737202
	1	−0.59617598	−0.60794575	−0.61078004	−0.54873672	0.07905123	0.4	0.37896055
$2s \to 3p$	0.1	1.53239528	1.56032134	1.57779183	1.51296821	0.96212776	0.01	0.43399889
	0.4	1.53239452	1.56024714	1.57830084	1.51388585	0.90876197	0.05	0.41594460
	0.5	1.53239406	1.56020449	1.57797157	1.51453142	0.88783614	0.1	0.36639711
	1	1.53239034	1.55987605	1.57652076	1.52043617	0.85542392	0.2	0.17105455
	Confined ECSCP						Free ECSCP	
Transition	λ_2	$r_c = 0.1$	$r_c = 0.5$	$r_c = 1$	$r_c = 2$	$r_c = 5$	λ_2	$r_c = \infty$
$1s \to 2p$	0.1	0.97072717	0.98455833	0.99105855	0.92726266	0.49020012	0.05	0.41541265
	0.5	0.97072715	0.98455130	0.99103661	0.92859601	0.39261746	0.1	0.41059123
	1	0.97072703	0.98450670	0.99091497	0.93723099	0.38873757	0.2	0.37680897
	1.4	0.97072679	0.98442680	0.99070952	0.95086935	0.72484192	0.25	0.33815629
$1s \to 3p$	0.1	0.02145205	0.00772596	0.00000215	0.04914057	0.25938284	0.01	0.07908337
	0.5	0.02145206	0.00773097	0.00000111	0.04772537	0.32705934	0.05	0.07727923
	1	0.02145216	0.00776310	0.00000195	0.03909999	0.33012451	0.1	0.06672974
	1.4	0.02145234	0.00782141	0.00003015	0.02603893	0.12347883	0.12	0.05778373
$2s \to 2p$	0.05	−0.59617948	−0.60825787	−0.61189909	−0.53993757	−0.07746440	0.05	0.00099592
	0.1	−0.59617948	−0.60825776	−0.61189792	−0.53993008	−0.07524706	0.1	0.00719122
	0.5	−0.59617945	−0.60824322	−0.61176097	−0.53953695	0.07707677	0.2	0.05235875
	1	−0.59617924	−0.60815247	−0.61102508	−0.54115043	0.16873325	0.25	0.10793827
$2s \to 3p$	0.05	1.53239533	1.56032654	1.57832534	1.51292362	0.96729789	0.01	0.43478301
	0.1	1.53239533	1.56032638	1.57832365	1.51291209	0.96572414	0.05	0.42653220
	0.5	1.53239529	1.56030638	1.57812514	1.51213836	0.84864260	0.1	0.37668282
	1	1.53239501	1.56018160	1.57705831	1.51229530	0.76798664	0.12	0.33241753
	SP							
Transition	$r_c = 0.1$	$r_c = 0.2$	$r_c = 0.5$	$r_c = 1$	$r_c = 2$	$r_c = 2.5$	$r_c = 5$	$r_c = 10$
$1s \to 2p$	0.97051035	0.97420550	0.98379490	0.99067302	0.92958863	0.84910611	0.46356524	0.40514594
$1s \to 3p$	0.02161960	0.01795866	0.00826516	0.00002030	0.04648691	0.10750364	0.27699337	0.10047172
$2s \to 2p$	−0.59580794	−0.59894650	−0.60667433	−0.60974041	−0.53810301	−0.45106011	−0.03771967	0.01415902
$2s \to 3p$	1.53188858	1.53916195	1.55815448	1.57522845	1.51008687	1.41740733	0.93835324	0.51932973

In WCP, the necessary expectation values will take the form

$$\langle \hat{T}\hat{V}\rangle_{n,\ell} = \left\langle \hat{T}\left(-\frac{Z}{r}e^{(-\lambda_1 r)}\right)\right\rangle_{n,\ell},$$
$$\langle \hat{V}\hat{T}\rangle_{n,\ell} = \left\langle \left(-\frac{Z}{r}e^{(-\lambda_1 r)}\right)\hat{T}\right\rangle_{n,\ell},$$
$$\langle \hat{V}^2\rangle_{n,\ell} = \left\langle \frac{Z^2}{r^2}e^{(-2\lambda_1 r)}\right\rangle_{n,\ell}, \quad \langle \hat{V}\rangle_{n,\ell} = \left\langle -\frac{Z}{r}e^{(-\lambda_1 r)}\right\rangle_{n,\ell}. \tag{49}$$

Now, applying the expression in Eq. (49) in Eq. (5), we obtain

$$\begin{aligned}\langle \hat{T}^2\rangle_{n,\ell} - \langle \hat{T}\rangle^2_{n,\ell} &= (\Delta\hat{T}_{n,\ell})^2 = \langle \hat{V}^2\rangle_{n,\ell} - \langle \hat{V}\rangle^2_{n,\ell} = (\Delta\hat{V}_{n,\ell})^2 \\ &= \left\langle \frac{Z^2}{r^2}e^{(-2\lambda_1 r)}\right\rangle_{n,\ell} - \left\langle \frac{Z}{r}e^{(-\lambda_1 r)}\right\rangle^2_{n,\ell} \\ &= \langle \hat{T}\rangle_{n,\ell}\left\langle -\frac{Z}{r}e^{(-\lambda_1 r)}\right\rangle_{n,\ell} - \left\langle \hat{T}\left(-\frac{Z}{r}e^{(-\lambda_1 r)}\right)\right\rangle_{n,\ell}. \end{aligned} \tag{50}$$

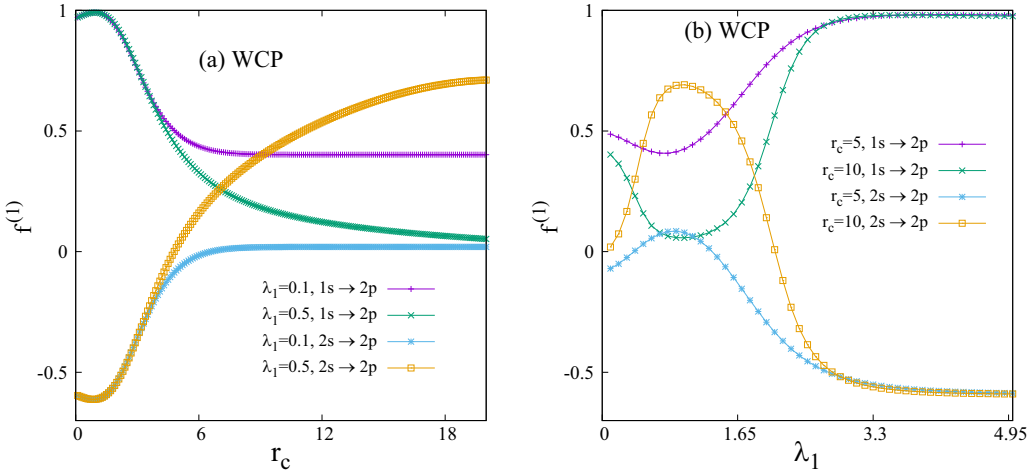

FIG. 4. $f^{(1)}_{ns\to 2p}(n=1,2)$ for WCP. (a) gives the r_c (in a.u.) variation at two selected λ_1 (0.1, 0.5 a.u.), while (b) shows the λ_1 (in a.u.) variation at two different r_c (5, 10 a.u.). See text for details.

The relevant expectation values in ECSCP are expressed as

$$\begin{aligned}
\langle \hat{T}\hat{V}\rangle_{n,\ell} &= \left\langle \hat{T}\left(-\frac{Z}{r}e^{(-\lambda_2 r)}\cos\lambda_2 r\right)\right\rangle_{n,\ell},\\
\langle \hat{V}\hat{T}\rangle_{n,\ell} &= \left\langle \left(-\frac{Z}{r}e^{(-\lambda_1 r)}\cos\lambda_2 r\right)\hat{T}\right\rangle_{n,\ell},\\
\langle \hat{V}^2\rangle_{n,\ell} &= \left\langle \frac{Z^2}{r^2}e^{(-2\lambda_2 r)}\cos^2\lambda_2 r\right\rangle_{n,\ell},\\
\langle \hat{V}\rangle_{n,\ell} &= \left\langle -\frac{Z}{r}e^{(-\lambda_2 r)}\cos\lambda_2 r\right\rangle_{n,\ell}. \qquad (51)
\end{aligned}$$

Now, substituting the results of Eq. (51) in Eq. (5), we achieve

$$\begin{aligned}
&\langle \hat{T}^2\rangle_{n,\ell} - \langle \hat{T}\rangle^2_{n,\ell}\\
&= (\Delta\hat{T}_{n,\ell})^2 = \langle \hat{V}^2\rangle_{n,\ell} - \langle \hat{V}\rangle^2_{n,\ell} = (\Delta\hat{V}_{n,\ell})^2\\
&= \left\langle \frac{Z^2}{r^2}e^{(-2\lambda_2 r)}\cos^2\lambda_2 r\right\rangle_{n,\ell} - \left\langle \frac{Z}{r}e^{(-\lambda_2 r)}\cos\lambda_2 r\right\rangle^2_{n,\ell}\\
&= \langle \hat{T}\rangle_{n,\ell}\left\langle -\frac{Z}{r}e^{(-\lambda_2 r)}\cos\lambda_2 r\right\rangle_{n,\ell}\\
&\quad - \left\langle \hat{T}\left(-\frac{Z}{r}e^{(-\lambda_2 r)}\right)\cos\lambda_2 r\right\rangle_{n,\ell}. \qquad (52)
\end{aligned}$$

In SP, the respective expectation values manifest as

$$\begin{aligned}
\langle \hat{T}\hat{V}\rangle_{n,\ell} &= \left\langle \hat{T}\left\{-\frac{Z}{r}+\frac{(Z-N_e)}{R}\left[3-\left(\frac{r}{R}\right)^2\right]\right\}\right\rangle_{n,\ell},\\
\langle \hat{V}\hat{T}\rangle_{n,\ell} &= \left\langle \left\{-\frac{Z}{r}+\frac{(Z-N_e)}{R}\left[3-\left(\frac{r}{R}\right)^2\right]\right\}\hat{T}\right\rangle_{n,\ell},\\
\langle \hat{V}^2\rangle_{n,\ell} &= \left\langle \left\{-\frac{Z}{r}+\frac{(Z-N_e)}{R}\left[3-\left(\frac{r}{R}\right)^2\right]\right\}^2\right\rangle_{n,\ell},\\
\langle \hat{V}\rangle_{n,\ell} &= \left\langle \left\{-\frac{Z}{r}+\frac{(Z-N_e)}{R}\left[3-\left(\frac{r}{R}\right)^2\right]\right\}\right\rangle_{n,\ell}. \qquad (53)
\end{aligned}$$

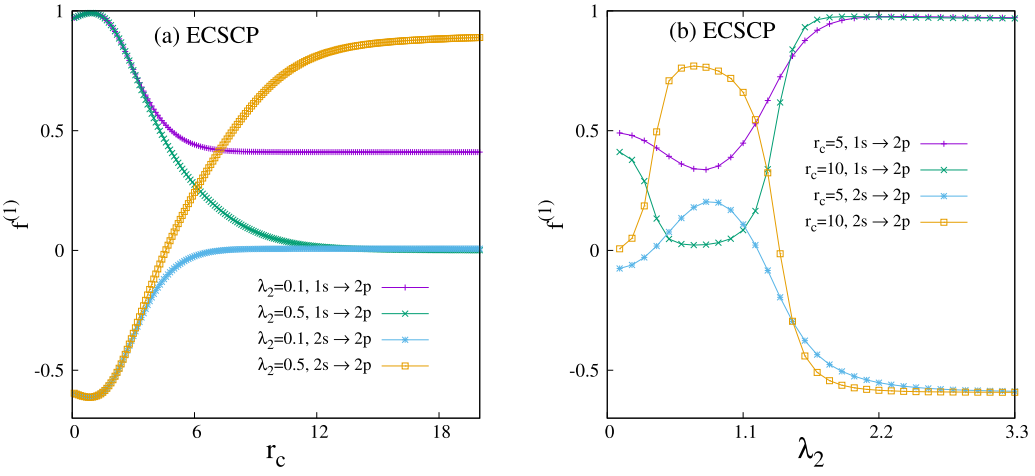

FIG. 5. $f^{(1)}_{ns\to 2p}(n=1,2)$ for ECSCP. (a) gives the r_c (in a.u.) variation at two selected λ_2 (0.1, 0.5 a.u.), while (b) shows the λ_2 (in a.u.) variation at two different r_c (5, 10 a.u.). See the text for details.

TABLE IV. $\alpha^{(1)}$ for WCP and ECSCP (in free and confined conditions) and SP in the 1s and 2s states.

	Confined WCP							Free WCP	
State	λ_1	$r_c=0.1$	$r_c=0.5$	$r_c=1$	$r_c=2$	$r_c=3$	$r_c=5$	λ_1	$r_c=\infty$
1s	0.1	0.00000348	0.00179958	0.02141842	0.14911950	0.25573621	0.28428984	0.05	0.2820913
	0.5	0.00000348	0.00180142	0.02159981	0.15905913	0.29929691	0.35670443	0.1	0.2845122
	1	0.00000348	0.00180662	0.02207243	0.18422797	0.43081698	0.66907982	0.2	0.2937360
	2	0.00000348	0.00182404	0.02347293	0.25795381	0.96822978	4.64009044	0.25	0.3004862
	2.5	0.00000348	0.00183517	0.02427643	0.29812432	1.30252206	8.89513209	0.3	0.3086925
	3	0.00000348	0.00184738	0.02509476	0.33616289	1.60942186	12.66519620	0.4	0.3297730
2s	0.1	0.000000784	0.00027589	−0.00105258	−0.30696765	−4.32610957	−150.21895140	0.05	4035.9536
	0.5	0.000000784	0.00027635	−0.00105258	−0.30187923	−4.62797003	503.53816745	0.1	1161.9265
	1	0.000000784	0.00027768	−0.00081299	−0.27873557	−4.40335922	287.82230501	0.2	419.04688
	2	0.000000784	0.00028251	−0.00020805	−0.19039680	−2.24216995	−53.18407330	0.25	339.24125
	2.5	0.000000784	0.00028579	0.00017337	−0.14358283	−1.42113266	−18.92337897	0.3	312.66238
	3	0.000000784	0.00028955	0.00058151	−0.10232148	−0.87783191	−8.40883662	0.4	393.94908
	Confined ECSCP							Free ECSCP	
State	λ_2	$r_c=0.1$	$r_c=0.5$	$r_c=1$	$r_c=2$	$r_c=3$	$r_c=5$	λ_2	$r_c=\infty$
1s	0.1	0.00000348	0.00179950	0.02141041	0.14867869	0.25393187	0.28156914	0.01	0.2812505
	0.5	0.00000348	0.00179980	0.02146640	0.15382762	0.28118411	0.33101794	0.05	0.2813193
	1	0.00000348	0.00180171	0.02178057	0.18029000	0.45239114	0.91168796	0.1	0.2817742
	1.25	0.00000348	0.00180359	0.02206630	0.20378040	0.65045235	2.57374006	0.2	0.2850410
	1.4	0.00000348	0.00180507	0.02227983	0.22117395	0.81774044	4.89195099	0.25	0.2883457
2s	0.1	0.00000078	0.00027587	−0.00105523	−0.30712416	−4.30664314	−136.34737101	0.01	89914.38
	0.5	0.00000078	0.00027591	−0.00104609	−0.30960540	−4.85239904	230.50804606	0.05	20470.3544
	1	0.00000078	0.00027620	−0.00098316	−0.30418590	−5.36027549	171.45198632	0.1	2954.0860
	1.25	0.00000078	0.00027650	−0.00091626	−0.28685821	−4.42905058	−831.87504495	0.2	546.52109
	1.4	0.00000078	0.00027674	−0.00086180	−0.27036124	−3.63524261	−91.86677448	0.25	386.92234
	SP								
State	$r_c=0.1$	$r_c=0.2$	$r_c=0.5$	$r_c=1$	$r_c=2$	$r_c=2.5$	$r_c=3$	$r_c=5$	$r_c=10$
1s	0.00000349	0.00005369	0.00183246	0.022259	0.160406	0.232152	0.273467	0.288320	0.282136
2s	0.00000078	0.00001131	0.00028033	0.011415	0.133172	0.275261	0.486354	2.354053	8.230057

Finally, engaging the outcome of Eq. (53) in Eq. (5) leads to

$$\begin{aligned}
&\langle\hat{T}^2\rangle_{n,\ell}-\langle\hat{T}\rangle^2_{n,\ell}\\
&=(\Delta\hat{T}_{n,\ell})^2=\langle\hat{V}^2\rangle_{n,\ell}-\langle\hat{V}\rangle^2_{n,\ell}=(\Delta\hat{V}_{n,\ell})^2\\
&=\left\langle\left\{-\frac{Z}{r}+\frac{(Z-N_e)}{R}\left[3-\left(\frac{r}{R}\right)^2\right]\right\}^2\right\rangle_{n,\ell}\\
&\quad-\left\langle\left\{-\frac{Z}{r}+\frac{(Z-N_e)}{R}\left[3-\left(\frac{r}{R}\right)^2\right]\right\}\right\rangle^2_{n,\ell}\\
&=\langle\hat{T}\rangle_{n,\ell}\left\langle\left\{-\frac{Z}{r}+\frac{(Z-N_e)}{R}\left[3-\left(\frac{r}{R}\right)^2\right]\right\}\right\rangle_{n,\ell}\\
&\quad-\left\langle\hat{T}\left\{-\frac{Z}{r}+\frac{(Z-N_e)}{R}\left[3-\left(\frac{r}{R}\right)^2\right]\right\}\right\rangle_{n,\ell}. \qquad (54)
\end{aligned}$$

The top part of Table II represents results for WCP in 1s and 2s states for six different sets of $\{\lambda_1, r_c\}$ values, namely, (0.1, 0.1), (0.1, 0.5), (0.5, 0.5), (1, 1), (1.5, 5), (0.45, ∞). In all these cases, Eq. (5) from Sec. II A is corroborated. More importantly, in a given state, at a fixed r_c, the energy increases with λ_1. Similarly, at a certain λ_1, it declines with a rise in r_c. In the middle part, the corresponding outcomes are tabulated for ECSCP at six chosen (λ_2, r_c) values, viz., (0.1, 0.1), (0.1, 0.5), (0.5, 0.5), (1, 1), (1.5, 5), (0.25, ∞). Again, these data support the conclusion drawn from Eq. (5). Like the WCP, here also, the energy increases with λ_2 at fixed r_c and diminishes with r_c at a specific λ_2. In the bottom part, numerical data about the validity of VT in the context of SP are presented. Like the earlier two cases, they also satisfy Eq. (5). It may be mentioned that a few attempts were made before to establish such a theorem in confined conditions (which includes the plasma environment) by means of the Hellmann-Feynman theorem and conventional VT [39,78]. There, the mathematical form of the expression changes from system to system; the present form, on the other hand, provides a uniform mathematical expression *irrespective of the system of interest*.

C. Multipole oscillator strengths and polarizabilities

In the following discussion, $Z=2$ is chosen; that means in SP β depends on only r_c. Hence, in SP, the results are provided with respect to variation of only r_c. It may be recalled from Sec. II C that in SP, Z is required to be greater than 1. That is why we have selected $Z=2$ instead of 1 for all three environments. Note that results for $Z=1$ in *free* WCP and ECSCP were also calculated. They are found to be in agreement with the available literature (see, e.g., [8,10] and

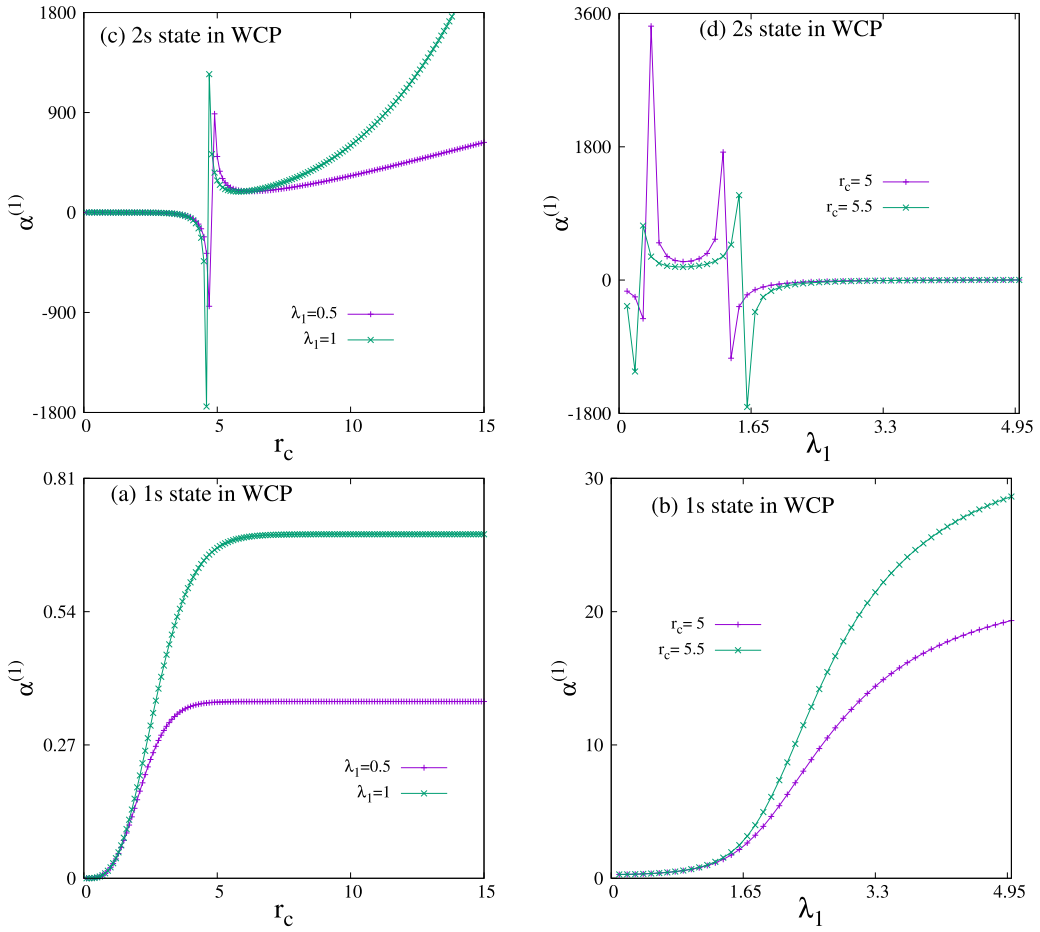

FIG. 6. $\alpha^{(1)}$ in $1s$, $2s$ states in WCP. (a) and (b) r_c (in a.u.) variation at two selected λ_1 (0.5, 1 a.u.) and (c) and (d) λ_1 (in a.u.) variation at two different r_c (5, 5.5 a.u.). See text for details.

references therein). In this work, the primary focus, however, is on *confined* plasma systems. The multipole OS sum rule given in Eq. (16) was estimated for both $1s$ and $2s$ states, involving all four k ($k = 1, 2, 3, 4$). In both free and confined conditions, this equation was obeyed. Further, this sum rule remains invariant under scaling transformations.

The OS, in practice, measures the probability of transition between an initial state and a final state. The dipole OSs for first two $\ell = 0$ states of WCP, ECSCP, and SP are presented in Table III. These changes do not seem to be straightforward. At $\lambda_1 \to 0$ (WCP) and $\lambda_2 \to 0$ (ECSCP), these results coalesce to a FHA. On the other hand, OS in SP approaches a FHA in the limit of $r_c \to \infty$. The selection rule is $\Delta\ell = \pm 1$; therefore, only p-wave states are permitted as final states. In all three cases, these are provided for $ns \to mp$ ($n = 1, 2; m = 2, 3$) states, in both free and confined conditions. In the *first two* plasma conditions, $f^{(1)}_{1s\to 2p}$ decreases in the strong-confinement regime ($r_c \leqslant 1$), with the rise in the screening constant, keeping r_c fixed. But for low to moderate r_c (1, 2) it increases with λ. However, at $r_c = 5$, it reduces to attain a minimum and then grows gradually. Interestingly, in the free condition, it again declines with the increase of λ. On the other hand, in either of the plasmas, at a fixed λ, it increases with r_c, then reaches a maximum, and eventually falls off. The positions of the maxima do not change with λ. In SP also, $f^{(1)}_{1s\to 2p}$ shows a similar behavior; it initially increases to reach a maximum and then declines. It can thus be stated that, in all three plasmas, there is an optimum T_e (refer to Sec. II C) at which the probability of transition attains a maximum. Moreover, with the growth in r_c and T_e, the plasma-tail effect predominates. At $r_c = 0.1$ and 0.5, only minor changes occur in $f^{(1)}_{1s\to 3p}$ with an increase in λ in both WCP and ECSCP. However, at $r_c = 1$, although the values are significantly small, nevertheless, there appears a minimum in $f^{(1)}_{1s\to 3p}$ versus λ plots for both plasmas. At $r_c = 2$, it decays with growth in λ. Further, at $r_c = 5$, there appears a maximum in the $f^{(1)}_{1s\to 3p}$ against λ_2 plot for ECSCP. However, in a similar plot for WCP, one finds a maximum followed by a minimum. On the contrary, at a fixed λ, in WCP and ECSCP with a rise in r_c, $f^{(1)}_{1s\to 3p}$ decreases to reach a minimum and then increases. But in SP, first, there occurs a minimum followed by a maximum. Thus, with a rise in T_e, the probability of transition from $1s$ to $3p$ decreases initially in all three potentials and increases thereafter. It is noticed that $f^{(1)}_{1s\to mp}(m = 2, 3)$ in free WCP and ECSCP decreases with an increase in λ.

Now, the focus is on the $2s$ states. Like in the previous case, here also, nontrivial variations are recorded in their change with r_c and λ. In this case, the occurrence of a negative sign in

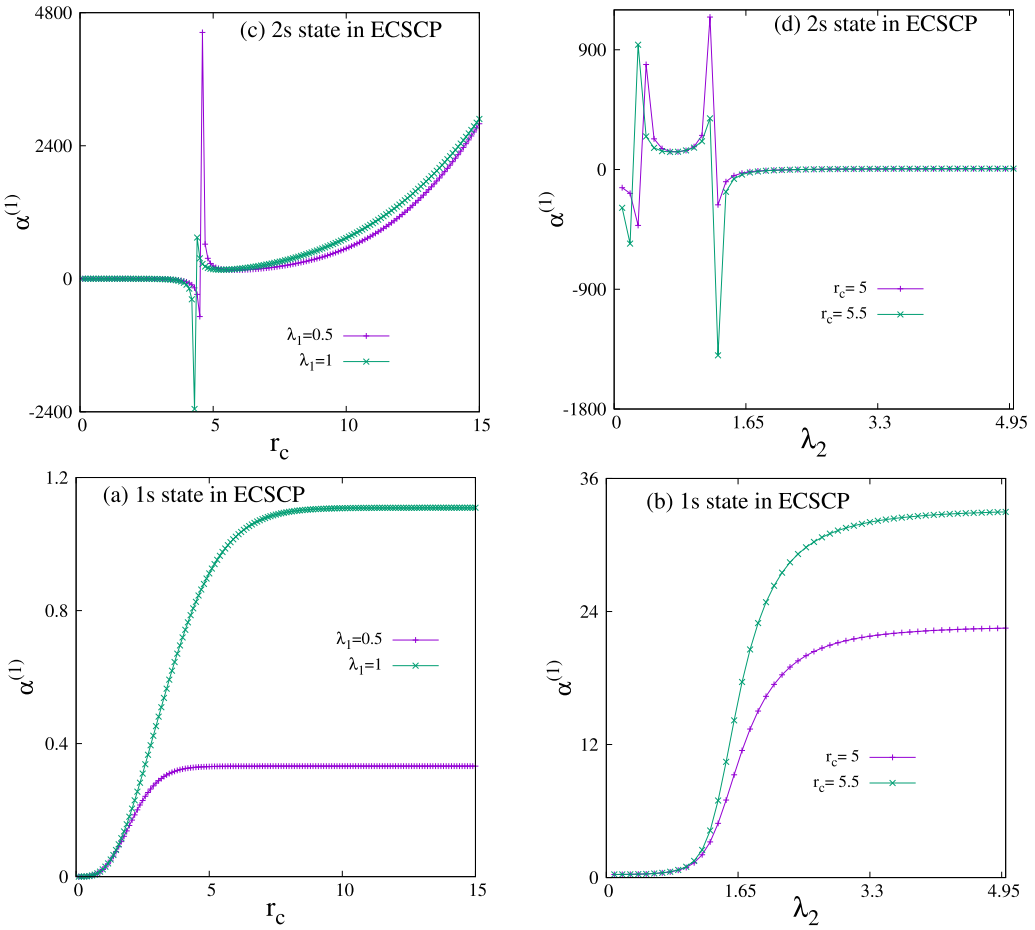

FIG. 7. $\alpha^{(1)}$ for ECSCP in 1s and 2s states. (a) and (b) r_c (in a.u.) variation at two selected λ_1 (0.5, 1 a.u.) and (c) and (d) λ_1 (in a.u.) variation at two different r_c (5, 5.5 a.u.). See text for details.

$f^{(1)}_{2s\to 2p}$ indicates emission. In WCP and ECSCP, at a fixed r_c in the strong-confinement region ($r_c \leqslant 2$), they remain almost unchanged with changes in λ. In this low-r_c region, emission occurs between these two states for all the λ considered. However, in $r_c = 5$, emission happens at lower values of λ. Thus, at this particular r_c, there appears a crossover between $\mathcal{E}_{2s}$ and $\mathcal{E}_{2p}$, with an increase in λ. The 2s to 3p transition provides the absorption spectrum. Similar to $f^{(1)}_{2s\to 2p}$, in the strong-confinement zone (at a fixed r_c), nominal changes occur in $f^{(1)}_{2s\to 3p}$ in both WCP and ECSCP. The same quantity, however, at $r_c = 5$, decreases with a rise in λ. At fixed λ, with a rise in r_c, it increases to reach a maximum and then decays. Similarly, in SP also, one gets a maximum with an increase in r_c at fixed λ. One observes that, in both WCP and ECSCP, $f^{(1)}_{2s\to mp}(m = 2, 3)$ decays with growth in λ. The results in Table III are graphically shown in Figs. 4 and 5 for confined WCP and confined ECSCP, respectively. Thus, $f^{(1)}_{ns\to 2p}(n = 1, 2)$ is plotted as a function of r_c at fixed λ and λ at given r_c in these plasma conditions. Two representative λ (5, 10) and r_c (0.1, 0.5) are chosen to illustrate these. There are certain similarities in the qualitative natures of these plots in Figs. 4(a) and 5(a), as well as in Figs. 4(b) and 5(b). From Figs. 4(a) and 5(a), one notices that, for both λ values, starting from a nonzero positive number, $f^{(1)}_{1s\to 2p}$ grows to a moderate extent, reaching a maximum at a lower r_c, and then sharply falls until converging to the respective free system. However, $f^{(1)}_{2s\to 2p}$ starts from a small negative number, then lowers to a slight extent to attain a minimum, and finally accelerates rapidly to reach the corresponding free limit in both WCP and ECSCP [also shown in Figs. 4(a) and 5(a)]. Next, Figs. 4(b) and 5(b) show $f^{(1)}_{1s\to 2p}$ gradually falls to a minimum from an initially positive number with an increase in λ and thereafter grows until reaching the free limit. As r_c increases, the plots display a well-like behavior with a flatter minimum, without any significant change in the positions of these minima. On the other hand, $f^{(1)}_{2s\to 2p}$ [again from Figs. 4(b) and 5(b)] initially shows a tendency to reach a maximum (which flattens with a rise in r_c) followed by a sharp fall to attain the FHA limit. All these patterns are not necessarily evident from Table III, which offers only a few entries to save space. Thus, one sees that 1s and 2s states maintain a complementary nature in Figs. 4 and 5.

Now, Table IV presents dipole polarizabilities $\alpha^{(1)}$ in 1s and 2s for all three plasmas. It retains the arrangement pattern in Table III, so the top, middle, and bottom parts contain results for WCP, ECSCP, and SP respectively. However, the chosen λ differ from those in Table III. At lower r_c ($\leqslant 0.5$), $\alpha^{(1)}_{ns}$ is quite small and remains practically unaltered with changes in λ. Similarly, in SP, it is also rather small. In the $r_c > 0.5$ region, however, $\alpha^{(1)}_{1s}$ continually increases with λ for a fixed r_c. Further, at a specific λ, it progresses with r_c. In

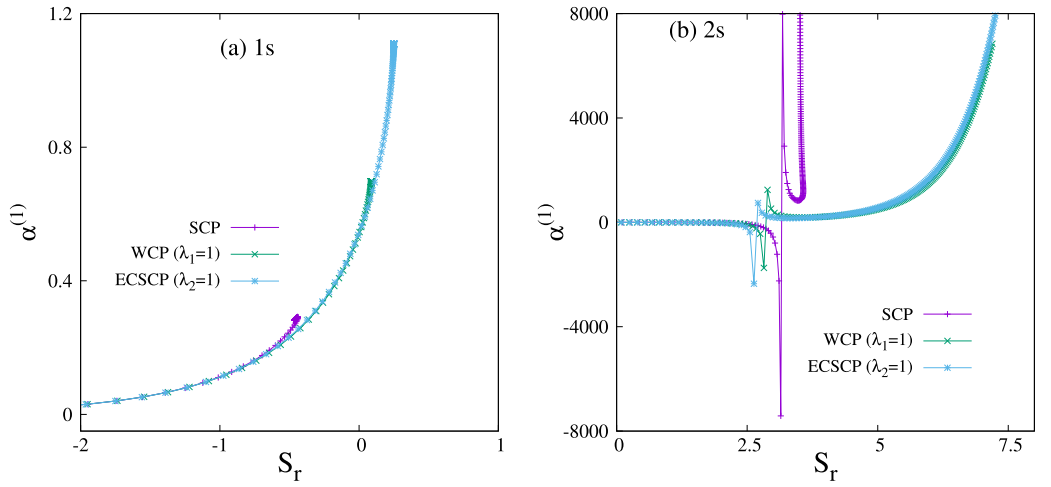

FIG. 8. Change in $\alpha^{(1)}$ with S_r in SP, WCP ($\lambda_1 = 1$ a.u.), and ECSCP ($\lambda_2 = 1$ a.u.) involving (a) $1s$ and (b) $2s$ states. See text for details.

essence, we conclude that, in the $1s$ state, with relaxation in confinement (increase in T_e) $\alpha^{(1)}$ increases. However, in the $2s$ state, $\alpha^{(1)}$ does not maintain the regular feature of the ground state. Thus, $\alpha^{(1)}_{2s}$ at $r_c = 0.5$ is higher than its counterpart in $r_c = 0.1$ for all λ. In WCP and ECSCP, it increases with λ at a constant r_c. At $r_c = 1$, in WCP $\alpha^{(1)}_{2s}$ attains a negative value at lower λ_1; with a rise in λ_1 it generally grows and eventually becomes positive towards the end. In contrast, in ECSCP it remains negative for all the λ_2 considered and slowly increases as we descend down the column. Further, at $r_c = 2$, 3, in both WCP and ECSCP, it reflects a negative value but, overall, increases with a rise in λ. Interestingly, however, at $r_c = 5$, in either WCP or ECSCP, it starts from an initially negative value at lower λ, then increases to a positive value, followed by a drop to attain a certain negative value again. These results have prompted us to investigate the behavior of $\alpha^{(1)}_{ns}$ as a function of λ, keeping r_c fixed at 5 and 5.5 in the corresponding plots (see Figs. 6 and 7). However, in SP, $\alpha^{(1)}_{ns}$ smoothly increases from a small number to reach a maximum and finally merge with FHA results (0.282136 and 7.5002 for $1s$ and $2s$). In free WCP and ECSCP, $\alpha^{(1)}_{1s}$ accelerates, while $\alpha^{(1)}_{2s}$ reduces, with growth in λ. These results are demonstrated in the last two columns.

The $\alpha^{(1)}_{ns}$ results in Table IV are depicted graphically in Figs. 6 and 7. Thus, Figs. 6(a) and 7(a) suggest that, at a fixed λ (0.5, 1), $\alpha^{(1)}_{1s}$ steadily increases with r_c until converging to the free limit. Figures 6(b) and 7(b) show that, at fixed r_c (5, 5.5), $\alpha^{(1)}_{1s}$ increases, initially slowly, but later sharply with λ, and then reaches the FHA limit. It is observed that, in either WCP or ECSCP, the numerical value of $\alpha^{(1)}_{1s}$ at $r_c = 5.5$ remains higher than that at $r_c = 5$. Similarly, the top rows of Figs. 6 and 7 provide the respective plots for $2s$ in WCP and ECSCP. From Figs. 6(c) and 7(c), it is inferred that, for a given λ (0.5, 1), $\alpha^{(1)}_{2s}$ records some abrupt fall to a high negative value at certain r_c, followed by a dramatic increase to a high positive value in a spikelike fashion, then again a drop, and, eventually, steady growth, thus giving rise to one maximum and minimum. On the contrary, at $r_c = 5$ or 5.5, in Figs. 6(d) and 7(d), it proceeds through two spikelike features with a change of sign in between high negative and high positive, passing through two maxima and minima. This complex pattern may occur due to a sign change in various energy states.

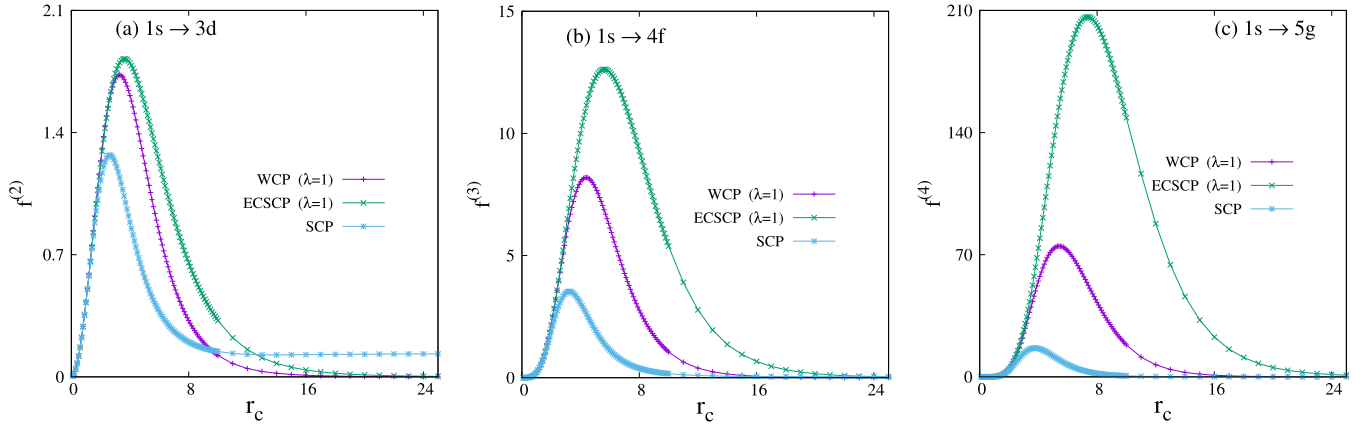

FIG. 9. Changes in (a) $f^{(2)}_{(1s\to 3d)}$, (b) $f^{(3)}_{(1s\to 4f)}$, and (c) $f^{(4)}_{(1s\to 5g)}$ with r_c (in a.u.) in WCP ($\lambda_1 = 1$ a.u.), ECSCP ($\lambda_2 = 1$ a.u.), and SP. See the text for details.

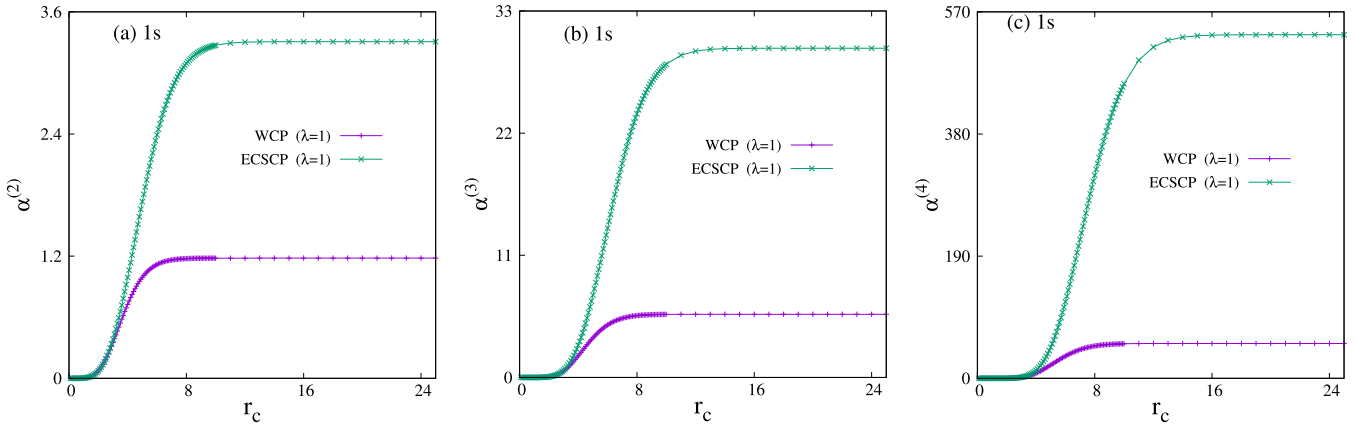

FIG. 10. Changes in (a) $\alpha^{(2)}$, (b) $\alpha^{(3)}$, and (c) $\alpha^{(4)}$ with r_c (in a.u.), involving the $1s$ state of WCP ($\lambda_1 = 1$ a.u.) and ECSCP ($\lambda_2 = 1$ a.u.). See the text for details.

From the above discussion it appears that the impact of confinement on $\alpha_{ns}^{(1)}$ $(n = 1, 2)$ is thought provoking. In order to probe it further, it would be interesting to invoke Shannon entropy. It is well known that S_r is an efficient measure of confinement [72,79]; with an increase of confinement strength S_r decreases, while S_r increases with its relaxation. Therefore, $\alpha^{(1)}$ is plotted as a function of S_r for both $1s, 2s$ states for all three plasmas. In WCP and ECSCP λ is kept fixed at 1. Figure 8(a) shows that, in all three cases, $\alpha_{1s}^{(1)}$ progress with S_r. But the dipole polarizability for $2s$ in Fig. 8(b) shows a behavior that is not so straightforward. Therefore, an in-depth analysis would be highly desirable.

Finally, some sample results are now presented for quadrupole, octupole, and hexadecapole OSs, as well as the polarizabilities involving WCP, ECSCP, and SP. The selection rules for these three different transitions are $\Delta\ell \pm 2, 3,$ and 4, respectively. To illustrate the qualitative features, we offer a cross section of these transitions, while detailed results will be published elsewhere. Figures 9(a)–9(c) show the variation of $f^{(2)}$, $f^{(3)}$, $f^{(4)}$, respectively, as a function of r_c for the three potentials for the $1s \rightarrow 3d$, $1s \rightarrow 4f$, and $1s \rightarrow 5g$ transitions. In WCP and ECSCP λ was chosen to be 1. For all three potentials, OS rises with r_c, then attains a maximum, and finally reaches the free values. This feature holds true for all the higher-order OSs. That means there exists a characteristic r_c at which the probability of the concerned transition is maximum. Similarly, Figs. 10(a)–10(c) displays changes in $\alpha^{(2)}, \alpha^{(3)}, \alpha^{(4)}$ with r_c in the $1s$ state for WCP and ECSCP. In both plasmas, $\alpha^{(k)}$ continually increases until it reaches a constant value corresponding to the free system. The analogous SP plots are qualitatively similar and thus are omitted.

IV. CONCLUSION

Multipole (up to order 4) OS and polarizabilities were probed for H-like ions in WCP, ECSCP, and SP. In the first two cases, the investigation was done in both free and confined conditions. A connection between T_e and r_c was proposed and analyzed. It was found that the plasma-tail effect can be controlled by introducing this confinement. Two generalized scaling ideas were derived connecting Z and λ separately. The relation between these two independent ideas was also achieved. Starting from a given Hamiltonian and using these designed relations, one can easily extract results for a series of Hamiltonians. An S_r-driven technique was designed to determine $\lambda_{n,\ell}^{(c)}$ for both WCP and ECSCP in the free environment accurately, where it increases stiffly. Further, using S_r-based results and this scaling idea, a generalized relation between $\lambda_{n,\ell}^{(c)}$ and Z was proposed which is applicable to an arbitrary state. The applicability of a recently proposed virial-like theorem was verified for the plasma systems studied here. Results were also presented for free WCP and ECSCP. A detailed investigation of these spectroscopic properties for $\ell \neq 0$ states would be highly desirable. The influence of the plasma-screening effect on the two-photon transition amplitude and photoionization cross section also needs to be explored in the confined condition. Other information-theoretic quantities like the Fisher information, Onicescu energy, complexity, mutual and relative information, etc., need to be examined. Exploration of the Hellmann-Feynman theorem in the context of confined plasma is necessary. A similar calculation in helium plasmas may provide vital insight into the effect of confinement on many-electron plasmas.

ACKNOWLEDGMENTS

Financial support from BRNS, India (Sanction Order No. 58/14/03/2019-BRNS/10255), is gratefully acknowledged. Partial financial support from SERB, India (CRG/2019/000293), is also appreciated. N.M. thanks CSIR, New Delhi, India, for a Senior Research Associateship (Pool No. 9033A). Critical constructive comments from two anonymous referees are greatly appreciated.

APPENDIX A: ANALYTICAL FORMS OF $f^{(k)}$ AND $\alpha^{(k)}$ IN FHA

The analytical expression for dipole polarizabilities in a FHA was reported in Ref. [80] for the $1s$ state. In this Appendix, we provide the 2^k-pole OS $(k = 1, 4)$ and respective polarizabilities for a FHA in both $1s, 2s$ states.

TABLE V. $\mathcal{E}_{n,0}$, $f^{(1)}_{ns\to 2p}$, and $\alpha^{(1)}_{ns}$ ($n = 1, 2$) values for three Hamiltonians, given in Eqs. (45). $\alpha^{(1)}_{ns}$ represents the bound-state polarizability. I signifies analytical results obtained by employing (a) Eqs. (25), (31), and (36) for $\mathcal{E}_{n,\ell}$, (b) Eqs. (27), (33), and (43) for $f^{(1)}_{js\to np}$, and (c) Eqs. (28), (34), and (44) for $\alpha^{(1)}_{ns}$. II indicates numerical results calculated using the Hamiltonian directly. $B = (\frac{2}{81})^{\frac{1}{3}}$.

	WCP											
	$H(1, 1, \frac{\lambda_1}{Z}, Zr_c, r_1)$				$H(1, \frac{Z}{\lambda_1}, 1, \lambda_1 r_c, r_2)$				$H(1, Z, \lambda_1, r_c, r)$			
$\frac{\lambda_1}{Z} = 2$,	$H(1, 1, 2, 1, r_1)$		$H(1, 1, 2, 2, r_1)$		$H(1, 0.5, 1, 2, r_2)$		$H(1, 0.5, 1, 4, r_2)$		$H(1, 1, 2, 1, r)$		$H(1, 2, 4, 1, r)$	
$r_c = 1$	$\lambda_1 = 2, Z = 1$		$\lambda_1 = 4, Z = 2$		$\lambda_1 = 2, Z = 1$		$\lambda_1 = 4, Z = 2$		$\lambda_1 = 2, Z = 1$		$\lambda_1 = 4, Z = 2$	
	I	II	I	II	I	II	I	II	I	II	I	II
$\mathcal{E}_{1,0}$	3.6923	3.6923	0.8644	0.8644	0.9230	0.9230	0.2161	0.2161	3.6923	3.6923	3.4576	3.4576
$f^{(1)}_{1s\to 2p}$	0.9825	0.9825	0.9877	0.9877	0.9825	0.9825	0.9877	0.9877	0.9825	0.9825	0.9877	0.9877
$\alpha^{(1)}_{1s}$	0.02998	0.02998	0.42689	0.42689	0.47968	0.47968	6.83026	6.83026	0.02998	0.02998	0.02668	0.02668
$\mathcal{E}_{2,0}$	17.8794	17.8794	4.2884	4.2884	4.4698	4.4698	1.07212	1.07212	17.8794	17.8794	17.1538	17.1538
$f^{(1)}_{2s\to 2p}$	−0.6051	−0.6051	−0.6039	−0.6039	−0.6051	−0.6051	−0.6039	−0.6039	−0.6051	−0.6051	−0.6039	−0.6039
$\alpha^{(1)}_{2s}$	0.00477	0.00477	0.02271	0.02271	0.07632	0.07632	0.36349	0.36349	0.00477	0.00477	0.00142	0.00142
	ECSCP											
	$H(1, 1, \frac{\lambda_1}{Z}, Zr_c, r_1)$				$H(1, \frac{Z}{\lambda_1}, 1, \lambda_1 r_c, r_2)$				$H(1, Z, \lambda_1, r_c, r)$			
$\frac{\lambda_1}{Z} = 2$,	$H(1, 1, 2, 1, r_1)$		$H(1, 1, 2, 2, r_1)$		$H(1, 0.5, 1, 2, r_2)$		$H(1, 0.5, 1, 4, r_2)$		$H(1, 1, 2, 1, r)$		$H(1, 2, 4, 1, r)$	
$r_c = 1$	$\lambda_1 = 2, Z = 1$		$\lambda_1 = 4, Z = 2$		$\lambda_1 = 2, Z = 1$		$\lambda_1 = 4, Z = 2$		$\lambda_1 = 2, Z = 1$		$\lambda_1 = 4, Z = 2$	
	I	II	I	II	I	II	I	II	I	II	I	II
$\mathcal{E}_{1,0}$	4.00195	4.00195	1.07647	1.07647	1.00048	1.00048	0.29612	0.29612	4.00195	4.00195	4.30589	4.30589
$f^{(1)}_{1s\to 2p}$	0.98265	0.98265	0.98488	0.98488	0.98265	0.98265	0.98488	0.98488	0.98265	0.98265	0.98488	0.98488
$\alpha^{(1)}_{1s}$	0.02998	0.02998	0.46172	0.46172	0.47981	0.47981	7.38750	7.38750	0.02998	0.02998	0.02885	0.02885
$\mathcal{E}_{2,0}$	18.1544	18.1544	4.47386	4.47386	4.53860	4.53860	1.11846	1.11846	18.15440	18.15440	17.89546	17.89546
$f^{(1)}_{2s\to 2p}$	−0.6047	−0.6047	−0.5971	−0.5971	−0.6047	−0.60477	−0.5971	−0.5971	−0.6047	−0.6047	−0.6047	−0.6047
$\alpha^{(1)}_{2s}$	0.00466	0.00466	0.02914	0.02914	0.07454	0.07454	0.46631	0.46631	0.00466	0.00466	0.00182	0.00182
	SP											
	$H(1, 1, (\frac{\sigma}{Z})^4, Zr_c, r_1)$				$H(1, \frac{Z}{\sigma}, 1, \sigma r_c, r_2)$				$H(1, Z, \sigma^4, r_c, r)$			
	$H(1, 1, \frac{1}{16}, 2, r_1)$		$H(1, 1, 1, 3B, r_1)$		$H(1, 2, 1, 1, r_2)$		$H(1, 1, 1, 3B, r_2)$		$H(1, 2, 1, 1, r)$		$H(1, 3, 3, B, r)$	
	$\sigma = 1, Z = 2$		$\sigma = 3, Z = 3$		$\sigma = 1, Z = 2$		$\sigma = 3, Z = 3$		$\sigma = 1, Z = 2$		$\sigma = 3, Z = 3$	
	I	II	I	II	I	II	I	II	I	II	I	II
$\mathcal{E}_{1,0}$	0.56979	0.56979	5.64694	5.64694	2.27917	2.27917	5.64694	5.64694	2.27917	2.27917	50.64694	50.64694
$f^{(1)}_{1s\to 2p}$	0.99067	0.99067	0.98176	0.98176	0.99067	0.99067	0.98176	0.98176	0.99067	0.99067	0.98176	0.98176
$\alpha^{(1)}_{1s}$	0.35614	0.35614	0.01769	0.01769	0.02226	0.02226	0.01769	0.01769	0.02226	0.02226	0.00021	0.00021
$\mathcal{E}_{2,0}$	3.99437	3.99437	24.2876	22.2876	15.97749	15.97749	24.2876	24.2876	15.97749	15.97749	218.5886	218.5886
$f^{(1)}_{2s\to 2p}$	−0.6097	−0.6097	−0.6048	−0.6048	−0.6097	−0.6097	−0.6048	−0.6048	−0.6097	−0.6097	−0.6048	−0.6048
$\alpha^{(1)}_{2s}$	−0.0149	−0.0149	0.00296	0.00296	−0.0009	−0.0009	0.00296	0.00296	−0.0009	−0.0009	0.000036	0.000036

The closed-form expressions for $f^{(1)}_{(1s\to np)}(Z)$ and $f^{(1)}_{(2s\to np)}(Z)$ are

$$f^{(1)}_{(1s\to np)}(Z) = \frac{2^8}{3Z^7}\, n^5\, \frac{(n-1)^{(2n-4)}}{(n+1)^{(2n+4)}},$$
$$f^{(1)}_{(2s\to np)}(Z) = \frac{2^{15}}{3Z^7}\, n^5\, (n^2-1)\, \frac{(n-2)^{(2n-5)}}{(n+2)^{(2n+5)}}. \quad \text{(A1)}$$

Now, applying Eq. (A1) in Eq. (7), one easily obtains $\alpha^{(1)}_i(\text{bound})(Z)$ for the $1s$ and $2s$ states of a FHA. They take the following forms:

$$\alpha^{(1)}_{1s}(\text{bound})(Z) = \sum_{i=2}^{n} \frac{2^{10}}{3Z^9}\, i^9\, \frac{(i-1)^{(2i-6)}}{(i+1)^{(2i+6)}},$$
$$\alpha^{(1)}_{2s}(\text{bound})(Z) = \sum_{i=2}^{n} \frac{2^{21}}{3Z^9}\, i^9\, (i^2-1)\, \frac{(i-2)^{(2i-7)}}{(i+2)^{(2i+7)}}. \quad \text{(A2)}$$

TABLE VI. $\lambda_{n,\ell}^{(c)}$ for H-like ions ($Z = 1$–4) for $3s$, $4s$, $4p$, $4f$, $5s$, $5p$, $5d$, $5f$, $5g$ states in WCP and ECSCP.

WCP				ECSCP			
Z	State	$\lambda_{n,\ell}^{(c)}$	$\mathcal{E}_{n,\ell}$	Z	State	$\lambda_{n,\ell}^{(c)}$	$\mathcal{E}_{n,\ell}$
1	$3s$	0.13656[a]	−0.00000013	1	$3s$	0.289685[b]	−0.00000005
2	$3s$	0.27614	−0.00000013	2	$3s$	0.217247	−0.00000014
3	$3s$	0.41563	−0.00000012	3	$3s$	0.144808	−0.00000026
4	$3s$	0.55510	−0.00000015	4	$3s$	0.072366	−0.00000009
1	$4s$	0.07636[a]	−0.00000020	1	$4s$	0.040407[b]	−0.00000015
2	$4s$	0.1554320	−0.00000001	2	$4s$	0.080838	−0.00000009
3	$4s$	0.23433	−0.00000002	3	$4s$	0.121266	−0.00000016
4	$4s$	0.31319	−0.00000005	4	$4s$	0.161693	−0.00000077
1	$4p$	0.06769[a]	−0.00000058	1	$4p$	0.03926[b]	−0.00000076
2	$4p$	0.13572	−0.00000025	2	$4p$	0.078526	−0.00000116
3	$4p$	0.20363	−0.00000116	3	$4p$	0.117789	−0.00000025
4	$4p$	0.271529	−0.00000076	4	$4p$	0.157053	−0.00000058
1	$4f$	0.04984[a]	−0.00000024	1	$4f$	0.035241[b]	−0.00000016
2	$4f$	0.099662	−0.00000014	2	$4f$	0.0704820	−0.00000064
3	$4f$	0.149493	−0.00000031	3	$4f$	0.1057237	−0.00000005
4	$4f$	0.199324	−0.00000056	4	$4f$	0.1409649	−0.00000019
1	$5s$	0.04822[a]	−0.00000024	1	$5s$	0.02578[b]	−0.00000016
2	$5s$	0.09921	−0.00000022	2	$5s$	0.051569	−0.00000065
3	$5s$	0.14991	−0.00000006	3	$5s$	0.077357	−0.00000065
4	$5s$	0.20054	−0.00000017	4	$5s$	0.103145	−0.00000024
1	$5p$	0.04471[a]	−0.00000001	1	$5p$	0.025313[b]	−0.00000039
2	$5p$	0.090253	−0.00000007	2	$5p$	0.05063	−0.00000068
3	$5p$	0.125506	−0.00000001	3	$5p$	0.075946	−0.00000083
4	$5p$	0.18071	−0.00000063	4	$5p$	0.101262	−0.00000064
1	$5d$	0.03996[a]	−0.00000002	1	$5d$	0.024499[b]	−0.00000037
2	$5d$	0.08004	−0.00000081	2	$5d$	0.049	−0.00000001
3	$5d$	0.120072	−0.00000007	3	$5d$	0.0735	−0.00000006
4	$5d$	0.160097	−0.00000002	4	$5d$	0.098	−0.00000010
1	$5f$	0.03538[a]	−0.00000055	1	$5f$	0.023482[b]	−0.00000008
2	$5f$	0.070778	−0.00000023	2	$5f$	0.046964	−0.00000035
3	$5f$	0.106168	−0.00000008	3	$5f$	0.0704464	−0.00000012
4	$5f$	0.141557	−0.00000038	4	$5f$	0.0939286	−0.00000006
1	$5g$	0.031343[a]	−0.00000006	1	$5g$	0.022371[b]	−0.00000029
2	$5g$	0.062687	−0.00000007	2	$5g$	0.0447428	−0.00000007
3	$5g$	0.09403	−0.00000056	3	$5g$	0.0671140	−0.00000056
4	$5g$	0.125374	−0.00000024	4	$5g$	0.0894856	−0.00000026

[a]Literature results for $\lambda_{n,\ell}^{(c)}$ [55,56]: (a) $\lambda_{3s}^{(c)} = 0.1394$, (b) $\lambda_{4s}^{(c)} = 0.07882$, (c) $\lambda_{4p}^{(c)} = 0.067885$, (d) $\lambda_{4f}^{(c)} = 0.049831$, (e) $\lambda_{5s}^{(c)} = 0.05058$, (f) $\lambda_{5p}^{(c)} = 0.045186$, (g) $\lambda_{5d}^{(c)} = 0.040024$, (h) $\lambda_{5f}^{(c)} = 0.035389$, and (i) $\lambda_{5g}^{(c)} = 0.031343$.

[b]Literature results for $\lambda_{n,\ell}^{(c)}$ [44,55,56]: (a) $\lambda_{3s}^{(c)} = 0.072436$, (b) $\lambda_{4s}^{(c)} = 0.040427$, (c) $\lambda_{4p}^{(c)} = 0.039263$, (d) $\lambda_{4f}^{(c)} = 0.035241$, (e) $\lambda_{5s}^{(c)} = 0.025787$, (f) $\lambda_{5p}^{(c)} = 0.025315$, (g) $\lambda_{5d}^{(c)} = 0.024500$, (h) $\lambda_{5f}^{(c)} = 0.023482$, and (i) $\lambda_{5g}^{(c)} = 0.022371$.

$f^{(2)}_{(1s\to nd)}(Z)$ and $f^{(2)}_{(2s\to nd)}(Z)$ are expressed as

$$f^{(2)}_{(1s\to nd)}(Z) = \frac{2^{12}}{5Z^9}\, n^7\,(n^2-4)\,\frac{(n-1)^{(2n-6)}}{(n+1)^{(2n+6)}},$$
$$f^{(2)}_{(2s\to nd)}(Z) = \frac{2^{27}}{5Z^9}\, n^7\,(n^2-1)\,\frac{(n-2)^{(2n-9)}}{(n+2)^{(2n+9)}}. \quad \text{(A3)}$$

Inserting Eq. (A3) in Eq. (7), one gets $\alpha_i^{(2)}(\text{bound})(Z)$ in the $1s$ and $2s$ states of a FHA as follows:

$$\alpha^{(2)}_{1s}(\text{bound})(Z) = \sum_{i=3}^{n} \frac{2^{12}}{5Z^{11}}\, i^{11}\,(i^2-4)\,\frac{(i-1)^{(2i-8)}}{(i+1)^{(2i+8)}},$$
$$\alpha^{(2)}_{2s}(\text{bound})(Z) = \sum_{i=3}^{n} \frac{2^{33}}{5Z^{11}}\, i^{11}\,(i^2-1)\,\frac{(i-2)^{(2i-10)}}{(i+2)^{(2i+10)}}. \quad \text{(A4)}$$

The analytical expressions for $f^{(3)}_{(1s\to nf)}(Z)$ and $f^{(3)}_{(2s\to nf)}(Z)$ are

$$f^{(3)}_{(1s\to nf)}(Z) = \frac{9}{7}\frac{2^{12}}{Z^{11}} n^9 (n^2-9)(n^2-4)\frac{(n-1)^{(2n-8)}}{(n+1)^{(2n+8)}},$$
$$f^{(3)}_{(2s\to nf)}(Z) = \frac{9}{7}\frac{2^{27}}{5Z^{11}} n^9 (n^2-9)(n^2+4)(n^2-1) \times \frac{(n-2)^{(2n-10)}}{(n+2)^{(2n+10)}}. \quad \text{(A5)}$$

Doing some mathematical manipulation after substituting Eq. (A5) into Eq. (7) yields $\alpha_i^{(3)}(\text{bound})(Z)$ for the $1s$ and $2s$ states of a FHA:

$$\alpha_{1s}^{(3)}(\text{bound})(Z) = \sum_{i=4}^{n} \frac{9}{7}\frac{2^{14}}{Z^{13}}\, i^{13}\,(i^2-9)(i^2-4) \times \frac{(i-1)^{(2i-10)}}{(i+1)^{(2i+10)}},$$
$$\alpha_{2s}^{(3)}(\text{bound})(Z) = \sum_{i=4}^{n} \frac{9}{7}\frac{2^{33}}{Z^{13}}\, i^{13}\,(i^2-9)(i^4+4)(i^2-1) \times \frac{(i-2)^{(2i-12)}}{(i+2)^{(2i+12)}}. \quad \text{(A6)}$$

Finally, $f_{(1s\to ng)}^{(4)}(Z)$ and $f_{(2s\to ng)}^{(4)}(Z)$ manifest as

$$f_{(1s\to ng)}^{(4)}(Z) = \frac{2^{18}}{9Z^{13}}\, n^{11}\,(n^2-16)(n^2-9)(n^2-4) \times \frac{(n-1)^{(2n-10)}}{(n+1)^{(2n+10)}},$$
$$f_{(2s\to ng)}^{(4)}(Z) = \frac{2^{39}}{9Z^{13}}\, n^{11}\,(n^2-16)(n^2-9)(n^2+2)^2(n^2-1) \times \frac{(n-2)^{(2n-12)}}{(n+2)^{(2n+12)}}. \quad \text{(A7)}$$

By inserting Eq. (A7) in Eq. (7) one may extract $\alpha_i^{(4)}(\text{bound})(Z)$ for $1s$, $2s$ with the form

$$\alpha_{1s}^{(4)}(\text{bound})(Z) = \sum_{i=5}^{n} \frac{2^{20}}{9Z^{15}}\, i^{15} \times (i^2-16)(i^2-9)(i^2-4)\frac{(i-1)^{(2i-12)}}{(i+1)^{(2i+12)}},$$
$$\alpha_{2s}^{(4)}(\text{bound})(Z) = \sum_{i=5}^{n} \frac{2^{45}}{9Z^{15}}\, i^{15}\,(i^2-16)(i^2-9)(i^2+2)^2 \times (i^2-1)\frac{(i-2)^{(2i-14)}}{(i+2)^{(2i+14)}}. \quad \text{(A8)}$$

APPENDIX B: SOME SELECTED RESULTS USING THE SCALING CONCEPT

Here, we demonstrate the derived relations presented in Sec. II D. Table V shows some sample results obtained by the proposed scaling concept. Here, we use these formulas to connect Z, λ, and r_c. However, they can be applied and extended to any Hamiltonian.

The top, middle, and bottom parts present results for WCP, ECSCP, and SP, respectively. In all three cases, the second and third, sixth and seventh, and 10th and 11th columns and fourth and fifth, eighth and ninth, and 12th and 13th columns form two separate groups. Here, due to lack of space, we restrict our calculation to three Hamiltonians. However, one can extend the number of such Hamiltonians in a given group by using this formulation. Interestingly, one can extract the results for all members of a particular group just by performing calculations for any one Hamiltonian belonging to that group.

APPENDIX C: $\lambda_{n,\ell}^{(c)}$ VALUES FOR HIGHER STATES IN WCP AND ECSCP

The critical screenings $\lambda_{n,\ell}^{(c)}$ of WCP and ECSCP for $Z =$ 1–4, in the $3s, 4s, 4p, 4f, 5s, 5p, 5d, 5f, 5g$ states are produced in Table VI.

[1] *Electronic Structure of Quantum Confined Atoms and Molecules*, edited by K. D. Sen (Springer, Cham, 2014).
[2] W. Jaskólski, Phys. Rep. **271**, 1 (1996).
[3] W. Grochala, R. Hoffmann, J. Feng, and N. W. Ashcroft, Angew. Chem., Int. Ed. **46**, 3620 (2007).
[4] E. Snider, N. Dasenbrock-Gammon, R. McBride, M. Debessai, H. Vindana, K. Vencatasamy, K. V. Lawler, A. Salammat, and R. P. Dias, Nature (London) **586**, 373 (2020).
[5] S. Ichimaru, Rev. Mod. Phys. **54**, 1017 (1982).
[6] J. C. Weisheit, Adv. At. Mol. Phys. **25**, 101 (1989).
[7] M. S. Murillo and J. C. Weisheit, Phys. Rep. **302**, 1 (1998).
[8] L. Zhu, Yu. Ying He, L. G. Jiao, Y. C. Wang, and Y. K. Ho, Phys. Plasmas **27**, 072101 (2020).
[9] S. Bhattacharyya, J. K. Saha, and T. K. Mukherjee, Phys. Rev. A **91**, 042515 (2015).
[10] L. G. Jiao, Y. Y. He, Y. Z. Zhang, and Y. K. Ho, J. Phys. B: At. Mol. Opt. Phys. **54**, 065005 (2021).
[11] M. Das, Phys. Plasmas **21**, 012709 (2014).
[12] A. Solyu, Phys. Plasmas **19**, 072701 (2012).
[13] S. Paul and Y. K. Ho, Phys. Plasmas **16**, 063302 (2009).
[14] M. K. Bahar and A. Solyu, Phys. Plasmas **21**, 092703 (2014).
[15] M. K. Bahar, A. Soylu, and A. Poszwa, IEEE Trans. Plasma Sci. **44**, 2297 (2016).
[16] F. A. Gutierrez and J. Diaz-Valdés, J. Phys. B **27**, 593 (1994).
[17] J.-S. Yoon and Y.-D. Jung, Phys. Plasmas **3**, 3291 (1996).
[18] S. Paul and Y. K. Ho, Phys. Plasmas **15**, 073301 (2008).
[19] S. Paul and Y. K. Ho, Phys. Rev. A **79**, 032714 (2009).
[20] Y.-D. Jung, Phys. Plasmas **2**, 332 (1995).
[21] Y.-D. Jung and J.-S. Yoon, J. Phys. B **29**, 3549 (1996).
[22] M. Y. Song and Y.-D. Jung, J. Phys. B: At. Mol. Opt. Phys. **36**, 2119 (2003).
[23] L. R. Zan, L. G. Ziao, J. Ma, and Y. K. Ho, Phys. Plasmas **24**, 122101 (2017).
[24] Y.-D. Jung, Phys. Plasmas **4**, 21 (1997).
[25] Y. Y. Qi, J. G. Wang, and R. K. Janev, Phys. Rev. A **80**, 063404 (2009).
[26] L. Liu and J. G. Wang, J. Phys. B **41**, 155701 (2008).
[27] L. Liu, J. G. Wang, and R. K. Janev, Phys. Rev. A **77**, 042712 (2008).
[28] A. Poszwa and M. K. Bahar, Phys. Plasmas **22**, 012104 (2015).
[29] B. Saha, P. K. Mukherjee, and G. H. F. Diercksen, Astron. Astrophys. **396**, 337 (2002).
[30] Y. Y. Qi, J. G. Wang, and R. K. Janev, Phys. Rev. A **78**, 062511 (2008).
[31] Y. Y. Qi, Y. Wu, J. G. Wang, and Y. Z. Qu, Phys. Plasmas **16**, 023502 (2009).
[32] Y. Y. Qi, J. G. Wang, and R. K. Janev, Phys. Rev. A **80**, 032502 (2009).

[33] M. Bassi and K. L. Baluja, Indian J. Phys. **86**, 961 (2012).
[34] B. Saha and P. K. Mukherjee, Phys. Lett. A **302**, 105 (2002).
[35] M. Das, Phys. Plasmas **19**, 092707 (2012).
[36] S. Kang, Y. C. Yang, J. He, F. Q. Xiong, and N. Xu, Cent. Eur. J. Phys. **11**, 584 (2013).
[37] J. K. Saha, T. K. Mukherjee, P. K. Mukherjee, and B. Fricke, Eur. Phys. J. D **62**, 205 (2011).
[38] C. Yadav, S. Lumb, and V. Prasad, Eur. Phys. J. D **75**, 21 (2021).
[39] H. E. Montgomery, Jr., K. D. Sen, and J. Katriel, Phys. Rev. A **97**, 022503 (2018).
[40] C. Stubbins, Phys. Rev. A **48**, 220 (1993).
[41] P. K. Shukla and B. Eliasson, Phys. Lett. A **372**, 2897 (2008).
[42] C. S. Lam and Y. P. Varshni, Phys. Rev. A **6**, 1391 (1972).
[43] C. S. Lai, Phys. Rev. A **26**, 2245 (1982).
[44] D. Singh and Y. P. Varshni, Phys. Rev. A **28**, 2606 (1983).
[45] R. Dutt, U. Mukherji, and Y. P. Varshini, J. Phys. B **19**, 3411 (1986).
[46] O. Bayrak and I. Boztosun, Int. J. Quantum Chem. **107**, 1040 (2007).
[47] S. Paul and Y. Ho, Comput. Phys. Commun. **182**, 130 (2011).
[48] I. Nasser, M. S. Abdelmonem, and A. Abdel-Hady, Phys. Scr. **84**, 045001 (2011).
[49] Y. Y. Qi, J. G. Wang, and R. K. Janev, Phys. Plasmas **23**, 073302 (2016).
[50] A. K. Roy, Int. J. Quantum Chem. **113**, 1503 (2013).
[51] H. F. Lai, Y. C. Lin, C. Y. Lin, and Y. K. Ho, Chin. J. Phys. **51**, 73 (2013).
[52] C. Y. Lin and Y. K. Ho, Eur. Phys. J. D **57**, 21 (2010).
[53] C. Y. Lin and Y. K. Ho, Comput. Phys. Commun. **182**, 125 (2011).
[54] S. Lumb, S. Lumb, and V. Prasad, Phys. Rev. A **90**, 032505 (2014).
[55] C. G. Diaz, F. M. Fernández, and E. A. Castro, J. Phys. A **24**, 2061 (1991).
[56] A. K. Roy, Int. J. Quantum Chem. **116**, 953 (2016).
[57] M. S. Murillo, Phys. Plasmas **11**, 2964 (2004).
[58] M. Belkhiri, C. J. Fontes, and M. Poirier, Phys. Rev. A **92**, 032501 (2015).
[59] Z.-B. Chen, H.-W. Hu, K. Ma, X.-B. Liu, X.-L. Guo, S. Li, B.-H. Zhu, L. Huang, and K. Wang, Phys. Plasmas **25**, 032108 (2018).
[60] D. Salzmann and H. Szichman, Phys. Rev. A **35**, 807 (1987).
[61] Y. Y. Qi, J. G. Wang, and R. K. Janev, Phys. Plasmas **24**, 062110 (2017).
[62] S. Sen, P. Mandal, P. K. Mukherjee, and B. Fricke, Phys. Plasmas **20**, 013505 (2013).
[63] N. Mukherjee and A. K. Roy, Phys. Rev. A **99**, 022123 (2019).
[64] A. K. Roy, Mod. Phys. Lett. A **29**, 1450104 (2014).
[65] A. K. Roy, J. Math. Chem. **52**, 1405 (2014).
[66] A. K. Roy, Mod. Phys. Lett. A **29**, 1450042 (2014).
[67] N. Mukherjee and A. K. Roy, J. Phys. B **53**, 235002 (2020).
[68] L. Zhu, Y. Y. He, L. G. Jiao, Y. C. Wang, and Y. K. Ho, Int. J. Quantum Chem. **120**, e26245 (2020).
[69] A. Dalgarno, Adv. Phys. **11**, 281 (1962).
[70] I. Bialynicki and J. Mycielski, Commun. Math. Phys. **44**, 129 (1975).
[71] R. Atre, A. Kumar, C. N. Kumar, and P. K. Panigrahi, Phys. Rev. A **69**, 052107 (2004).
[72] N. Mukherjee and A. K. Roy, Int. J. Quantum Chem. **118**, e25596 (2018).
[73] L. G. Jiao, L. R. Zan, Y. Z. Zhang, and Y. K. Ho, Int. J. Quantum Chem. **117**, e25375 (2017).
[74] R. C. Estañón, N. Aquino, D. Puertas-Centeno, and J. S. Dehesa, Int. J. Quantum Chem. **120**, e26192 (2020).
[75] C. Martínez-Flores, Phys. Lett. A **386**, 126988 (2021).
[76] S. J. C. Salazar, H. G. Laguna, B. Dahiya, V. Prasad, and R. P. Sagar, Eur. Phys. J. D **75**, 127 (2021).
[77] A. Ghoshal and Y. K. Ho, Phys. Rev. E **81**, 016403 (2010).
[78] J. Katriel and H. E. Montgomery, Jr., J. Chem. Phys. **137**, 114109 (2012).
[79] N. Mukherjee and A. K. Roy, Adv. Theory Simul. **1**, 1800090 (2018).
[80] A. C. Tanner and A. J. Thakkar, Int. J. Quantum Chem. **24**, 345 (1983).